Safety Science 191 (2025) 106938

Contents lists available at ScienceDirect

Safety Science

journal homepage: www.elsevier.com/locate/safety

Transmission of SARS-CoV-2 via larger respiratory droplets in A restaurant environment

Zhaozhi Wang, Fuchen Jia, Edwin R Galea *, John Ewer, Angus Grandison

Fire Safety Engineering Group (FSEG), Centre for Safety, Resilience and Protective Security (CSRPS), University of Greenwich, UK

ARTICLE INFO

Keywords:
COVID-19
Restaurant environment
CFD
Wells-Riley model
Larger droplet
Ventilation
Table partition

ABSTRACT

A coupled Wells-Riley and CFD modelling technique utilising a multi-size droplet approach is adopted to investigate the transmission route in a COVID-19 infection event. The event occurred in a restaurant in China during 2020 and involved a single suspected index patient and 88 other patrons.

Using a multi-size droplet approach involving droplets up to 40 μm and a back-calculated quanta generation rate, nine secondary infections are predicted in the infection region, as in actual event. Furthermore, in the non-infection region, seating 68 susceptibles, an additional 1.7 infections are predicted. This compares with 23.3 infections when using the aerosol modelling approach (1 μm droplets). It is also estimated, using tracer gas data from an experiment conducted in this restaurant and simulation data using a small droplet model (5 μm), both reported in the literature, that there would be 22.0 and 6.1 infections respectively, within the non-infection region.

Thus, from these studies, only the multi-size droplet model, with droplets up to 40 μm can produce a reasonable estimation of the number of secondary infections. This suggests that the transmission of SARS-CoV-2 in this event is dominated by larger droplets, not aerosols or small droplets. The study also suggests that for this event, high ventilation rates alone are not an appropriate mitigation. This research challenges the findings of other researchers that infections in this event were due to small droplets and poor ventilation. Furthermore, table partitions and restricting dining duration are demonstrated to mitigate infection risk, reducing secondary infections by over 50 %.

1. Introduction

The COVID-19 pandemic, caused by the transmission of the SARS-CoV-2 virus, has claimed more than 7.1 million lives with more than 777.1 million people known to have been infected worldwide (World Health Organization (WHO) and Coronavirus, 2025) (at the time of writing in January 2025). Restaurants have been one of the high-risk indoor environments for COVID-19 transmission due to the impracticality of mask-wearing, potential high occupancy and localised population density, asymptomatic staff moving around serving patrons, surface contamination, potentially poor ventilation etc. Through monitoring of indoor air quality in a large cruise ship while at sea, Cheung et al. (Cheung et al., 2024) suggest that bars and restaurants potentially have higher infection risk than other public spaces. Statistical research based on data from 11 academic health care facilities by Fisher et al. (Fisher et al., 2020) reveals that patients with positive SARS-CoV-2 test results were approximately twice as likely to have reported dining at a restaurant as those with negative SARS-CoV-2 test results. In the state of Wisconsin, USA, 1633 (or 12.1 %) of reported cases were infected in restaurants and bars (Pray et al., 2021). A COVID-19 outbreak in a poorly ventilated restaurant (identified here and by Li et al. (Li et al., 2021) as the X restaurant) in Guangzhou China, occurred on the 24th January 2020 (Lu et al., 2020; Li et al., 2021), in which one suspected index patient is reported to have caused nine secondary infections amongst the other 88 patrons. On the 17th June 2020, there was an outbreak in a restaurant in Korea, in which one index patient is reported to have caused three secondary infections among 13 susceptible diners (Kwon et al., 2020). On the 25th July 2020, an infected staff member (index) is reported to have caused 19 secondary infections in a restaurant in Sydney, Australia (Capon et al., 2021). In another restaurant transmission event, occurring in Hong Kong on the 19th February 2021, before the enhancement of indoor air dilution was introduced, an infected patron is reported to have caused 31 secondary infections amongst 21 of 76 patrons and 10 of 19 staff (Cheng et al., 2022; Jia et al., 2024). In a later restaurant transmission event in Hong Kong that

* Corresponding author.
E-mail address: E.R.Galea@gre.ac.uk (E.R. Galea).

https://doi.org/10.1016/j.ssci.2025.106938
Received 2 March 2025; Received in revised form 24 June 2025; Accepted 25 June 2025
Available online 1 July 2025

Nomenclature

a	Number of quanta contributed from fomites contact
c	Quanta concentration (quanta/m^3)
d	Droplet diameter (m)
i	Droplet group number
p	Infection probability (%)
q	Quanta generation rate (quanta/h)
t	Exposure time (h)
v	Pulmonary ventilation rate of each susceptible (m^3/h)
$\overrightarrow{v}_i$	Settling velocity of group i droplet (m/s)
I	Number of index patients
N	Number of secondary infections
Q	Room ventilation rate (m^3/h)
RIR	Reported infection region
RNIR	Reported non-infection region
Y	Scalar variable
C_d	Droplet mass concentration (kg/m^3)
F_d	Droplet deposition rate on solid surface (kg/m^{2}s)
S_Y	Source term of scalar Y (kg/m^{3}s)
V_d	Droplet deposition velocity (m/s)
Y_i	Mass fraction of droplet group i
$\overline{C}$	Normalised gas concentration
$\overline{E}$	Normalised droplet exposure
α	Coefficient of normalised gas concentration
β	Coefficient of normalised droplet exposure
ρ	Air density (kg/m^3)
ρ_d	Droplet density (kg/m^3)
λ	The expectation of the Poisson distribution

occurred after the enhancement of indoor air dilution, one index patient is reported to have caused seven secondary infections among 207 susceptible people on the 27th December 2021 (Cheng et al., 2022). On the 23rd May 2021, one index patient caused nine secondary infections in another restaurant in Guangzhou, China (Zhang et al., 2022).

The SARS-CoV-2 virus can be transmitted between infected and susceptible individuals via the route of fomites (surface contamination) and through the air via droplet- or aerosol- transmission, as reported in studies during the early stages of the COVID-19 pandemic (Greenhalgh et al., 2021; Meyerowitz et al., 2020; Kampf et al., 2020). The distinction between droplet and airborne transmission is often based on a cut-off droplet diameter, most commonly taken to be 5 μm. Drossinos et al. (Drossinos et al., 2021) suggest that this traditional droplet-aerosol dichotomy is no longer tenable in view of the extensive theoretical and experimental work on respiratory droplets. They suggest that this arbitrary dichotomy is replaced by a unique non-contact airborne transmission mode. In this way, the two traditional airborne transmission mechanisms (i.e., via droplets or aerosol) are merged into a single airborne transmission mode (World Health Organization., 2024). As commented by Reid et al. (Reid et al., 2024), the merger of the two traditional airborne transmission mechanisms represents significant progress in collating the understanding of infectious respiratory disease transmission following collective research efforts during COVID-19. However, the explicit use of the term aerosol provides a nuanced, accepted and scientifically rigorous term that implicitly captures the imprecise boundaries of, for example, the variability in particle mechanics with size. In this study, for clarity in comparing our results with previous studies of the same infection event, and highlighting the specific transmission mode in the investigated infection event, the terms aerosol and droplet are used throughout the paper to distinguish between the study approaches. If appropriate and effective mitigation measures for reducing SARS-CoV-2 transmissions in restaurants are to be taken, it is important to first identify the dominant transmission routes in these settings. A methodology of combining the Wells-Riley epidemiological model (Wells, 1955; Riley et al., 1978) and the Computational Fluid Dynamics (CFD) simulation technique (Patankar, 1980; Hathway et al., 2011; Peng and Liu, 2020; Mirzaie et al., 2021; Coldrick et al., 2022) has been applied to estimate infection probabilities via airborne transmission (Wang et al., 2021; Zhu et al., 2012; Yan et al., 2017). While the technique applied by Wang et al. (Wang et al., 2021) was used to explore aerosol transmission events, it can also be adapted to explore transmission via larger droplets and can be utilised to determine possible dominant transmission routes. In the analysis presented in this paper, this modelling technique is used to determine the likely dominant transmission route in the X restaurant infection event in China. In this case, all nine secondary infections were seated either at the table with the index patient or at two neighbouring tables (identified as the 'reported infection region' or RIR) (Li et al., 2021). However, there were no secondary infections at the other 15 tables (identified as the 'reported non-infection region' or RNIR) as indicated in Fig. 1.

The transmission routes in the infection event at the X restaurant have been investigated by several researchers. Zhang et al. (Zhang et al., 2021) examined security video data from the restaurant taken at the time of the infection event and observed more than 40,000 surface touches and 13,000 episodes of close contacts. The term 'close contact' is intended to represent possible transmission routes that occur when the index and susceptible are in close physical proximity to each other (with separation distances of less than 2 m) and includes mechanisms such as

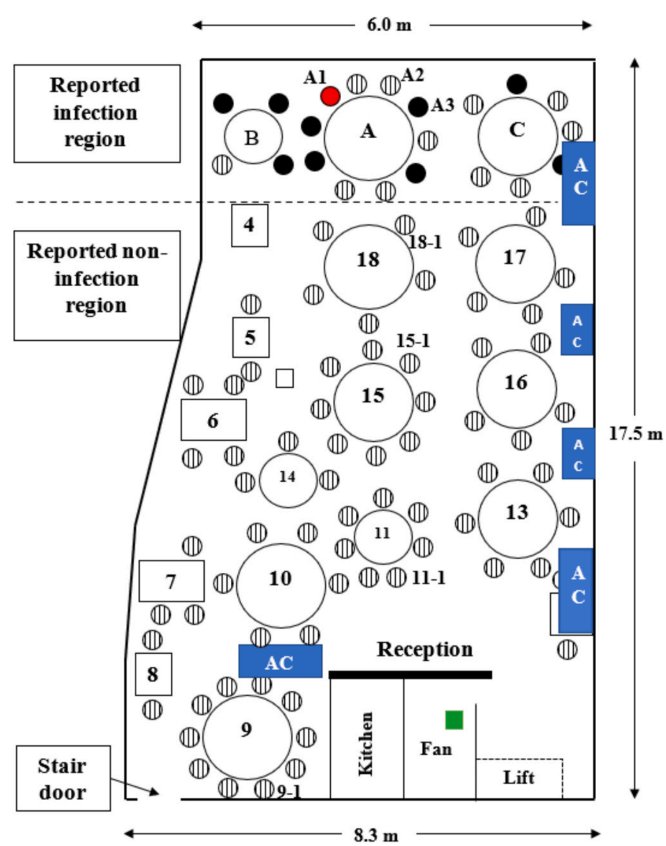

Fig. 1. Floor plan of the restaurant showing air conditioner units (AC); location of the index patient (A1) and location of secondary infections (black circles). Circles filled with lines represent susceptibles. (note: the small square located between table 5, table 6 and table 15 is a column).

short range airborne transmission by large droplets. As such, their study provides valuable information on people's surface touching behaviour while dining. However, they rule out virus transmission via contact with surface fomites and interpersonal close contact routes by comparing the surface touching behaviours between the infected and the non-infected patrons. Liu et al. (Liu et al., 2021) have used the aerosol exposure derived from CFD simulations to provide a spatial map of the airborne infection risk in the X restaurant under different air conditioning and thermal settings. Their results suggest a direct linkage between regions of high aerosol exposure and the reported infection patterns in the RIR. Unfortunately, the infection risk map at the other 15 tables (i.e., the RNIR) was not reported in the paper and so it is not possible to determine if they also predicted infections in other regions. In the work of Li et al. (Li et al., 2021), while they did not predict the number of secondary infections in the X restaurant infection event, using experimental and numerical analysis they investigated the infection risk for all the patrons based on the measured tracer-gas concentrations and simulated droplet (5 μm) exposure. These investigations (Li et al., 2021; Zhang et al., 2021; Liu et al., 2021) suggest that poor ventilation in the restaurant is the likely root cause of the transmission of the SARS-CoV-2 viral infection in the X restaurant, not close contact between patrons or surface touching.

The previous investigations of the X restaurant infection event using CFD simulation (Li et al., 2021; Liu et al., 2021) have clearly demonstrated the high infection risk in the RIR through the air flow pattern and the measured or simulated airborne particle distributions. However, none of these studies could explain why there were no secondary infections in the RNIR within the poorly ventilated restaurant. One major concern in these previous modelling studies is the particle sizes used in the CFD simulations for the X restaurant event. As reviewed by Stettler et al. (Stettler et al., 2022), during talking, the exhaled particle size distributions vary from 0.1 μm to hundreds of μm. The CFD simulation by Liu et al. (Liu et al., 2021) adopted a particle size of 1.5 μm, while that of Li et al. (Li et al., 2021), used droplets with a size of 5 μm. The aerosol approach (using droplets of less than around 1 μm) or droplet approach using small particle size (usually no more than 5 μm) in CFD simulations is based on the 'known' phenomenon of droplet drying, which can occur in a timescale of approximately 1 s (Stettler et al., 2022). However, this very short drying time is derived for water droplets. In contrast, it has been found that respiratory droplets, including those containing corona viruses, can last much longer than previously thought (Chong et al., 2021; Lieber et al., 2021; Pease et al., 2022). The study by Pease et al. (Pease et al., 2022) shows that mucus shells increase the drying time of respiratory droplets by orders of magnitude so that enveloped virions may remain well hydrated and, thus, fully infective for significantly longer periods of time and hence travel substantially greater distances. They conclude that the mucus in droplets provides a mechanism by which infective enveloped virus particles can transmit as aerosols within buildings and between buildings over extended distances. For example, the time to completely dry a 20 μm pure water droplet at 25 ^{O}C and a humidity of 80 % is approximately 1 s. In contrast, the drying time for a 20 μm core–shell mucus particle with a wet shell is approximately three hours. Mucus rich droplets are commonly emitted from the lungs, larynx, and oral cavities. The conclusion drawn by Pease et al. is important, especially for the SARS-CoV-2 transmission in restaurant environments. If larger droplets, in particular those with mucus shells, can survive for a long period of time, SARS-CoV-2 transmission through these larger droplets cannot be ignored. Therefore, larger size droplets i.e., larger than aerosol sized particles, should be considered in the investigations of SARS-CoV-2 transmission to fully understand transmission mechanisms. Furthermore, as the very large droplets do not rapidly evaporate forming a fine aerosol (or smaller particles), they cannot be carried long distances on air currents infecting susceptibles far from the index. Thus, there is a range of respiratory particle size, between that of aerosol size i.e., around 1 μm and the very large size i.e., of the order of 100 μm, that should be considered in transmission events where the susceptibles are located far from the index patient. In this study, this range of droplet sizes is referred to as 'larger droplets'.

In this study, through the investigation of the transmission event at the X restaurant, the possible effect of larger droplets in SARS-CoV-2 transmission is examined. This study numerically investigates this transmission event using a coupled CFD simulation and Wells-Riley modelling technique (Wang et al., 2021; Zhu et al., 2012; Yan et al., 2017). The CFD simulation is carried out by adopting a multi-size large droplets approach. The settling of droplets is modelled with the drift flux model (Chen et al., 2006; Hu et al., 2017; Overholt et al., 2016). In Section 2 it is demonstrated that the transmission event in the X restaurant was unlikely to have been via aerosols or small droplets. The investigation methodology used in this study, including some model validation are described in Section 3. The CFD modelling setup is presented in Section 4 followed by the simulation results analysis. The results are further discussed in Section 5 by comparing predictions produced in this work with some modelling work involving larger droplet sizes by other researchers; analysing the sensitivity of droplet size; interpreting the high quanta generation rate by considering surface deposition of large droplets; discussing the potential infection risk via surface contact and exploring mitigation measures including social distancing, ventilation rate and table partition etc. Limitations of the analysis are discussed in Section 6. Finally, conclusions are drawn in Section 7.

2. Can aerosol transmission explain the X restaurant infection event?

In this section, the SARS-CoV-2 infection event within the X restaurant is described. Experimental tracer gas dispersion data and CFD modelling results derived from the study by Li et al. (Li et al., 2021) are used to estimate the likely number of secondary infections. This analysis is used to demonstrate that aerosol dispersion alone cannot explain the X restaurant infection event.

2.1. The X restaurant infection event

The infection event occurred in the X restaurant in Guangzhou China on the 24th January 2020 (Lu et al., 2020; Li et al., 2021). The restaurant, located on the third floor of the building, had a floor plan as shown in Fig. 1. At the time of the infection event there were 89 patrons seated at 18 tables with the suspected index patient, identified as A1, seated at table A (Li et al., 2021) (see Fig. 1). The meal service duration for the index patient was 82 min. The exposure times of other patrons, starting from the arrival of the index patient were between 48 and 89 min with an average of 72 min (for details see Table 3). There was a central air conditioning system including five air supply units. However, the air conditioning system only recirculated air within the restaurant i.e., did not bring in fresh air from outside, and had an air filtration efficiency of 20 % (Li et al., 2021). An exhaust fan was in operation within the rest room. The stair door and the lift to the restaurant opened occasionally during the infection event. In total, there were nine secondary infections reported in the X restaurant event, all of which were clustered together and seated at table A, table B and table C. The region in which all the secondary infections occur is identified as the 'reported infection region' (RIR) in Fig. 1. It is noted that there were no secondary infections reported at the other 15 tables in the restaurant. This region is identified as the 'reported non-infection region' (RNIR) in Fig. 1.

2.2. Secondary infections based on data from the literature

The X restaurant infection event has been experimentally studied using ethane as the tracer gas, and numerically simulated using 5 μm particles by Li et al. (Li et al., 2021). The normalised gas concentrations derived from the experimental data and the normalised droplet exposure derived from the modelling results, for each table, are represented in the

Supplementary Material (SM), Table S1 in Section S1. The normalised concentration at a dining table is the average concentration measured at the table in the experiment divided by the measured average concentration at table A, where the index patient was seated. The droplet exposure at each table is the product of the simulated average droplet concentration at the table and the exposure duration. The normalised droplet exposure at a table is the droplet exposure at the table divided by the droplet exposure at table A.

The Wells-Riley model (Riley et al., 1978) (see Eq. (1)) determines the infection probability under a given ventilation condition in a confined space and is given by,

$$p = 1 - e^{-\lambda} = 1 - e^{-Iqvt/Q} \quad (1)$$

where λ is the parameter of Poisson distribution, which is the number of inhaled quanta by a susceptible; p is the infection probability; I is the number of index patients (in the infection event considered in this study, $I = 1$); v is the pulmonary ventilation rate of each susceptible (m^3/h); Q is the ventilation rate (m^3/h) of the confined space; q is the quanta generation rate produced by one index patient (quanta/h); and t is the exposure time (h). It should be noted that a well-mixed condition is assumed for the Wells-Riley model.

The Wells-Riley model (Eq. (1)) has also been interpreted as a dose–response model by many researchers e.g., Buonanono et al. (Buonanno G., Morawska L. et al., 2020; Buonanno G., Stabile L. et al., 2020). When interpreted in this way, a quantum is defined as the dose of airborne droplet nuclei required to cause infection in 63 % of susceptible persons. In this work, the dose definition of quantum is adopted. In Eq. (1), $Iqvt/Q$ is the cumulative inhaled quanta, which is proportional to the normalised gas concentration $\overline{C}$ and normalised droplet exposure $\overline{E}$ in Table S1 in SM Section S1. Therefore, Eq. (1) can be expressed as follows;

$$p = 1 - e^{-\alpha\overline{C}} \quad (2)$$

$$p = 1 - e^{-\beta\overline{E}} \quad (3)$$

where α and β are coefficients related to $\overline{C}$ and $\overline{E}$ respectively.

Using the known number of susceptibles and the actual number of secondary infections in the RIR, coefficients α and β can be back calculated and have been determined to be 0.619 and 0.0088 respectively (see SM Section S1). With these coefficient values, while correctly producing 9 secondary infections in the RIR, there are also predicted to be 22.0 secondary infections in the RNIR based on the tracer gas experimental data and 6.1 secondary infections based on the particle simulation (i.e., using 5 μm droplets) results (see SM Table S1 in Section S1).

While both the aerosol (i.e., tracer gas) experiment and the small droplet (i.e., 5 μm) simulation of this transmission event by Li et al. correctly produced higher normalised gas concentrations and normalised droplet exposures in the RIR than that in the RNIR, they fail to explain why no secondary infections occurred in the RNIR during this event. This suggests that aerosol transmission and transmission by small droplets alone cannot explain the X restaurant infection event. Hence, the small droplet transmission approach cannot represent the dominant transmission route in the X restaurant infection event.

In the remainder of this paper, the infection event in the X restaurant is investigated using the coupled Wells-Riley and CFD simulation modelling technique involving the multi-size droplet approach.

3. Models

The coupled Wells-Riley model and CFD simulation technique (Wang et al., 2021) is briefly described in this section. The drift flux and deposition models for particle transportation are also validated using experimental data (see section 3.4 and SM Section S2).

3.1. CFD model

SMARTFIRE V5.1 (Wang et al., 2021; Ewer, 2017; Wang et al., 2017; Grandison et al., 2006; Wang et al., 2001) was used to perform the airflow simulations in this study. The CFD engine in SMARTFIRE (Ewer et al., 2017) has been described in the literature many times and so only a brief description is provided here. SMARTFIRE has many physics features that are required for airflow modelling, such as mass, momentum, energy, and species conservation. Turbulence is modelled using the two-equation κ-ε model with buoyancy modification (Galea, 1989).

Along with the usual CFD transport equations required to accurately model the bulk- and local- air flows (Patankar, 1980; Ewer et al., 2017), the SMARTFIRE CFD software uses a simplified transportation model to represent the quanta dispersal. The model utilises a scalar tracer gas to represent the spread of respired aerosols from an index patient as expressed in Eq. (4):

$$\frac{\partial \rho Y}{\partial t} + \nabla \bullet \left(\rho \overrightarrow{U} Y\right) = \nabla \bullet (\varepsilon \nabla Y) + S_Y \quad (4)$$

where Y stands for a scalar, ε is the effective turbulent diffusivity, $-S_Y$ is the source term of Y, and $\overrightarrow{U}$ is the air velocity. In this study, Y is a dimensionless variable representing the mass fraction of exhaled aerosols within the mixture of ambient air and exhaled aerosols. In this study, Eq. (4) is used in the droplet approach.

In the CFD analysis presented in this paper, the settling of droplet particles is modelled with the drift flux model (Hu et al., 2017; Hu et al., 2011). The droplets are divided according to their sizes into a number of groups with an average diameter size of d_i for the i^{th} group. The transport of the droplet particles in the i^{th} group is defined by a governing equation:

$$\frac{\partial \rho Y_i}{\partial t} + \nabla \bullet (\rho(\overrightarrow{U} + \overrightarrow{v}_i)Y_i) = \nabla \bullet (\varepsilon \nabla Y_i) + S_{Y_i} \quad (5)$$

where Y_i denotes the mass fraction of the i^{th} droplet group. $\overrightarrow{v}_i$ is the settling velocity of the representative droplet in the group. The settling velocity $\overrightarrow{v}_i$ has the same direction as the gravity. The settling velocity is given by Eq. (6):

$$|\overrightarrow{v}_i| = \frac{g(\rho_d - \rho)d_i^2}{18\mu} \quad (6)$$

where g is the magnitude of the gravitation acceleration. ρ_d is the droplet density. μ is the viscosity of the fluid. d_i is the representative particle size of the droplet group. The total droplet mass fraction, Y, is given by Eq. (7):

$$Y = \sum Y_i \quad (7)$$

The deposition rate of droplets on per unit solid surfaces, F_d, is modelled with the approach proposed in (Liljegren et al., 2016), given by Eq. (8):

$$F_d = C_d \times V_d \quad (8)$$

where C_d is the droplet mass concentration and V_d is the deposition velocity.

Eqs. (5) to (8) are used in this study in the multi-size droplet approach in which particle sizes vary in a specific range.

3.2. Modified Wells-Riley model

The Wells-Riley model Eq. (1) is modified to couple the CFD simulation results to produce infection probability based on the modelled droplet concentrations. With a given quanta generation rate q (quanta/h) and pulmonary ventilation rate v (m^3/h), the quanta concentration in the flow generated from the breath of an index patient is q/v quanta/m^3.

The scalar value of the tracer gas, discussed previously, in the breathing stream of the index patient, is set to 1. If the average scalar value in a target volume is Y, the quanta concentration in this volume is then obtained with equation:

$$c = \frac{qY}{v} \tag{9}$$

The quanta concentration in Eq. (9) is based on the assumption that the quanta of droplets is proportional to their volume or mass. This hypothesis is assumed in the quanta generation rate derivation by Buonanno et al. (Buonanno G., Stabile L. et al., 2020). Therefore, taking $I = 1$ for the case with only one index patient and replacing Iq/Q in Eq. (1) with c, the local infection probability based on the CFD simulation is calculated using Eq. (10):

$$p = 1 - e^{-cvt} \tag{10}$$

In this work, for simplicity, it was assumed that the index patient and all the susceptibles have the same pulmonary ventilation rate. This leads to the cancellation of the pulmonary ventilation rate term in Eq. (10) when Equation (9) is substituted into Eq. (10).

If the quanta concentration is transient, the infection probability given by Eq. (10) can be recast to Eq. (11) with the accumulative inhaled quanta:

$$p = 1 - e^{-v\int_0^t cdt} \tag{11}$$

In addition to the inhaled quanta by respiration, if the quanta taken by fomites contact is considered, the infection probability (11) can be further extended to Eq. (12):

$$p = 1 - e^{-a-v\int_0^t cdt} \tag{12}$$

where a is the number of quanta contributed from fomites contact. With the individual infection probability p_j for susceptible j, N, the number of the secondary infections within a susceptible group, is given in Eq. (13) (Riley et al., 1978):

$$N = \sum_j p_j \tag{13}$$

3.3. Quanta generation rate

The quanta generation rate is one of the essential parameters when the Wells-Riley model (Riley et al., 1978) is applied to assess the infection risk in confined spaces. Quanta generation rate is thought to be dependent on the infectivity of the index patient and the nature of the activity they are involved in, e.g. breathing while resting, breathing while involved in light/heavy activity, speaking or coughing etc. As a result, a wide variety of quanta generation rates are suggested or derived from data of various COVID-19 transmission events. For the original SARS-CoV-2 variant, Buonanno et al. (Buonanno G., Morawska L. et al., 2020) have provided a variety of quanta generation rates. This included breathing (while resting), breathing (during heavy activity), speaking (during light activity), singing/speaking loudly (during light activity), with average quanta generation rates of 0.37, 2.5, 5.0 and 32 quanta/h respectively. However, it has been shown that many superspreader events have quanta generation rates as high as hundreds of quanta/h (Buonanno G., Morawska L. et al., 2020; Buonanno G., Stabile L. et al., 2020; Miller et al., 2021; Wang et al., 2021). The quanta generation rate of 100 quanta/h, derived from superspreader events, has been used in the analysis of SARS-CoV-2 transmission by Wang et al. (Wang et al., 2021), Pease et al. (Pease et al., 2021) and Marcus et al. (Marcus, et al., 2020).

Furthermore, as the SARS-CoV-2 virus mutates, the quanta generation rate must be revaluated to represent the infectivity of the mutated virus variant. The SARS-CoV-2 variant B1.1.7 mutation is reported to be between 40 % and 70 % more transmissible than the original variant (Volz et al., 2021). The B.1.617.2 variant is reported to be between 26 % and 115 % more transmissible than the B1.1.7 variant (Dagpunar, 2021; Allen et al., 2022; Campbell et al., 2021). From the first report of the Omicron variant (B.1.1.529) of SARS-CoV-2 in November 2021, infected cases increased rapidly around the world (Classification of Omicron, 2011). For this more infective Omicron variant, based on back-calculation for a restaurant spread event, the quanta generation rate is approximately 1023 quanta/h (Cheng et al., 2022). The derivation of the quanta generation rate for the transmission event in the X restaurant is described in Section 4.2.

3.4. Model validation

The coupled Wells-Riley and CFD simulation technique described here, has been validated using COVID-19 infection data from Chinese long-distance trains by Wang et al. (Wang et al., 2021), in which the spread of aerosols generated from index patients was simulated with the transportation of a tracer gas. In the multi-size droplet approach used in the current study, although larger droplets are involved, they are still modelled as a tracer gas, but with the settling and deposition characteristics of larger droplets addressed by the drift flux and deposition models described in section 3.1. Some validation of the version of the model representing larger droplet sizes (i.e., the multi-size particle drift model) is provided before the model is applied to simulate droplet distributions in the X restaurant transmission event. The experimental data used to validate the model is based on data measured in a model room environment (Chen et al., 2006). The details of the validation study can be found in the SM, Section S2. Presented in Fig. 2 is a comparison of measured and predicted concentrations of 10 μm particles at various heights at distances of 0.2 m, 0.4 m, and 0.6 m from the inlet. As seen in Fig. 2, the simulated particle concentrations are in good agreement with the measured data. These results suggest that the SMARTFIRE CFD model with drift flux and deposition models is able to simulate the dispersion of moderately large droplets in a ventilated room.

4. CFD simulations and estimation of secondary infections

In this section, the SARS-CoV-2 transmission route in the X restaurant is investigated using coupled CFD and Wells-Riley models with the dispersion modelling being simulated utilising both the aerosol and multi-size droplet approaches. The transmission mechanism that best describes the X restaurant infection event is identified, producing the correct secondary infection rate in the reported infection region (RIR) and minimal secondary infections in the reported non-infection region (RNIR).

4.1. Simulation setup

Two types of simulation are conducted, one using the aerosol approach and the other using the multi-size droplet approach. It is reported that the index patient did not display any symptoms during the infection event (i.e., the lunch event) until she returned to the hotel after the event (Li et al., 2021). It is also reported that the diners in the X restaurant spent approximately 21.9 % of the time speaking (Xu et al., 2024). As this was considered the most significant activity for generating aerosol droplets, the respiratory droplet data for talking is utilised in this study. As identified by Stettler et al., the range of respiratory droplet sizes exhaled during talking vary from less than 1 μm to hundreds of μm (Stettler et al., 2022). As part of the numerical simulations, it is necessary to determine the appropriate droplet size distribution to represent within each type of simulation.

For the aerosol approach, the droplet size is typically assumed to be of the order of 1 μm as larger respiratory droplets are assumed to rapidly evaporate and shrink to droplet nuclei of some final size dependent on their composition. This is also the droplet size used in the aircraft cabin

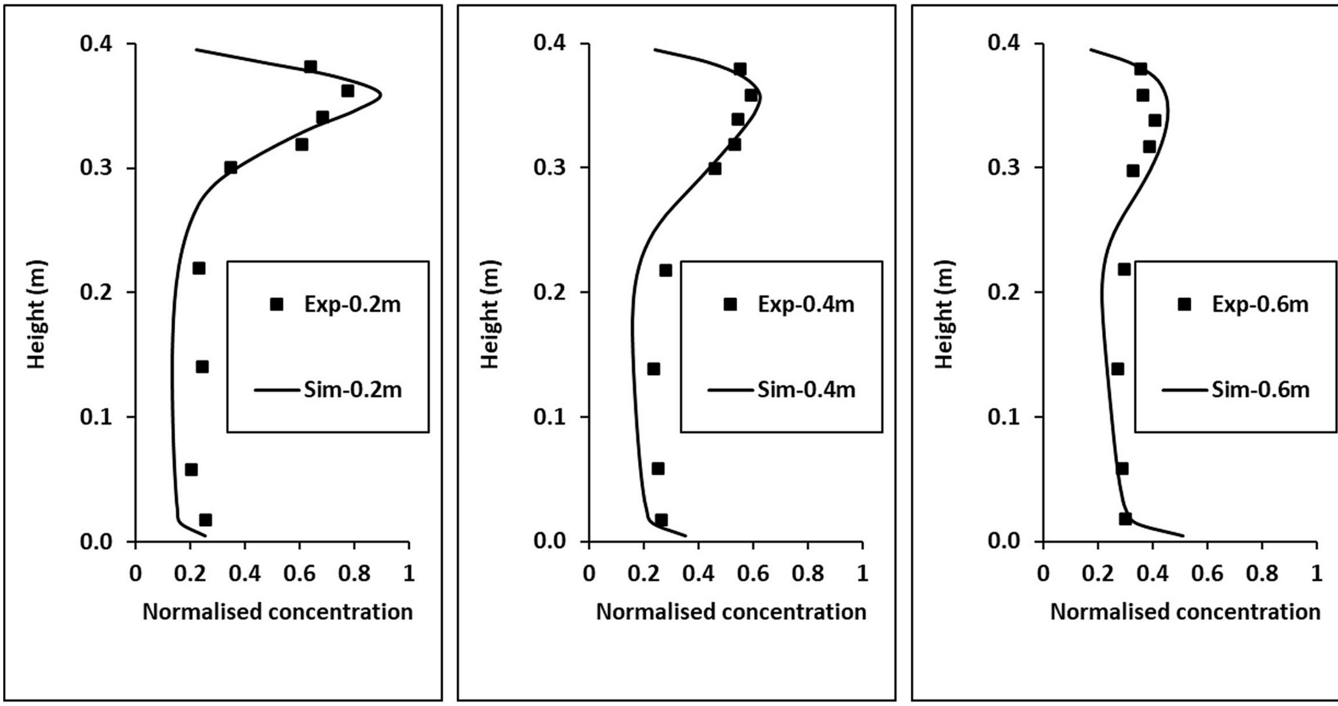

Fig. 2. Comparison of measured and simulated concentrations of 10 μm particles at three vertical lines (monitoring stacks) with 0.2 m, 0.4 m, and 0.6 m to the inlet respectively.

droplet dispersion experiment conducted by Silcott et al. (Silcott et al., 2020) and furthermore, is close to the particle size of 1.5 μm used in the investigation of the X restaurant transmission event by Liu et al. (Liu et al., 2021). Thus, for the aerosol model described in this paper, a droplet size of 1 μm is assumed. For the multi-size droplet approach, it is assumed that the time required for the larger droplets to evaporate is significantly greater than the exposure time and so the larger droplets persist. Thus, using this approach, a range of particle sizes is represented within the model, varying from aerosol sized particles (i.e., less than 5 μm) to moderately sized particles (approximately 5 μm to approximately 40 μm) to large droplets (greater than approximately 40 μm).

For the X restaurant infection event, the exposure time over which the infections occurred is of the order of 82 min. The assumption that the larger respiratory particle size droplets persist in the air flow is supported by research, including that of Pease et al. (Pease et al., 2022) and Lieber et al. (Lieber et al., 2021). Pease et al. (Pease et al., 2022) derived a correlation between the evaporation time and particle size and humidity for mucus containing droplets. They found that 20 μm droplets can persist for as long as three hours if they are mucus rich and the environmental humidity is 80 %. Pease et al. concluded that infective enveloped virus particles can transmit as aerosols within buildings and between buildings over extended distances. Mucus rich droplets are commonly emitted from the lungs, larynx, and oral cavities. From levitation experiments and numerical modelling, Lieber et al. (Lieber et al., 2021) found that complete evaporation of saliva droplets does not occur, and their airborne lifetime greatly increases in comparison to that of pure water droplets. They found that saliva droplets with an initial diameter of less than 50 μm may stay airborne for more than one hour. These findings are important because public health agencies typically follow the Wells' observation to establish health policies including social/physical distancing guidelines (Pease et al., 2022). Wells found that 200 μm water droplets will evaporate within 6.6 s in unsaturated air at 18 °C and the evaporation time is only 0.5 s for 50 μm water droplets (Wells, 1934). However, this approach fails to take into consideration that the droplets are not simply water but contain mucus. Furthermore, the region where the X restaurant is located has high humidity, with a year-average humidity of 78 % (Average humidity in Guangzhou, 2022) however, the indoor humidity level during the event at the restaurant is unknown. Assuming that the humidity levels within the restaurant were high during the event, the droplet sizes during this transmission event could have been as large as the droplets originally emitted by the index patient.

The size range and mass distribution of particles emitted by the index patient must be estimated for the multi-size droplet approach. Firstly, the maximum likely size of the large droplets is determined numerically. Very soon after being emitted, large droplets rapidly fall under gravity and deposit on surfaces such as the floor or tabletops – they are thus unlikely to be a vector for infection transmission at large distances from the index patient. From several initial simulations, it was found that droplets with a size of no greater than 37.5 μm can be transported from the location of the index patient i.e., seat A1, to the neighbouring tables B and C (see SM Section S3), before the normalised droplet concentration (normalised with the droplet concentration at the source i.e., index patient) decays by 99.95 %. Secondly, the mass distribution for the larger droplets is derived from measured particle number data. Using security video footage, it has been estimated that during the transmission event in the X restaurant, diners spent approximately 21.9 % of the time speaking (Xu et al., 2024). In an experiment by Xie et al., (Xie et al., 2009), the number and size distribution of respiratory particles produced by test participants while talking and coughing was measured. Data from three test participants (two males and one female), were collected in the talking experiments using food dye and sugar (to stimulate secretion of saliva and decrease droplet evaporation) and the data from these experiments are used to produce an average number of droplets within each particle size range. While the food dye and sugar did not influence the size distribution of droplets produced, more droplets were generated, and this may be a good approximation for the droplet size distribution produced while talking during dining. Given the earlier observation that particles of less than approximately 37.5 μm will travel beyond the incident table, in this study, the average droplet distributions measured by Xie et al., (Xie et al., 2009) up to a maximum of 40 μm have been adopted.

Finally, the droplet sizes and corresponding mass compositions derived from the counted droplet numbers in the experiment are presented in Table 1. The droplet mass in each size group is calculated using its representative diameter. In the mass composition calculation, the total droplet mass is calculated for all the droplets within the selected range, i.e. up to a maximum of 40 μm derived from the three trial participants.

For various size droplets, their deposition onto solid surfaces must be addressed within CFD simulations. For particles with size greater than 1 μm, the deposition velocity to horizontal surfaces is dominated by the particle size and the nature of the surface properties (Giardina and Buffa, 2018; Lai and Nazaroff, 2000). The adopted deposition velocity of each size group of droplets is shown in Table 1. They are estimated from the curves for sticky wood surfaces in the work by Giardina et al. (Giardina and Buffa, 2018) (it is assumed that surfaces within the restaurant environment, such as dining tables, are likely to be sticky and the environment is likely to have high humidity). These deposition velocities are applied to surfaces such as the floor, tables and patron clothes in this study.

The assumed air conditioner particle filtration efficiencies for the various particle sizes used in this study are listed in Table 1. The filtration efficiency of the air conditioner units in the X restaurant was reported by Li et al. (Li et al., 2021) to be 20 %. However, it is unknown what droplet size this efficiency relates to. Filtration efficiency for particles with size between 3 μm and 10 μm is on average 60 % for common air conditioner filers in UK trains (Anozie et al., 2020). Considering that filtration efficiency decreases as particle size decreases, it is assumed that the filtration efficiency for the air conditioner units in the X restaurant is 5 % for the 2.5 μm droplet group and 60 % for 7.5 μm droplet group used in this study. The efficiencies for droplet groups with sizes greater than 10 μm are assumed to be 95 % (Table 1). The filtration efficiency of air conditioners used in restaurants are usually not high for aerosol particles. Therefore, the filtration efficiency for aerosols (1 μm) is assumed to be 5 % (Table 2).

Other key model parameters and their values are summarised in Table 2. The COVID-19 infection event within the X restaurant occurred in the very early stages of the pandemic. At this time, the impact of ventilation on infection risk was not widely known. Therefore, a low air change rate of 4.9 ACH (air change per hour) is assumed for the restaurant. A constantly open vent measuring 0.6 m wide and 0.2 m high at the bottom of the stair door is used to represent the ventilation produced by the door that is occasionally opened. The flow rate of 0.072 m^3/s for the exhaust fan in the restroom is equivalent to the natural ventilation rate, which is estimated to be 0.56–0.77 ACH (Li et al., 2021). The model parameters for the inlets/outlets of the air conditioner units, the exhaust fan in the restroom and the boundary conditions are described in Table 2. The room temperature is assumed to be 20 °C. As the air conditioner units only recirculate air, the fresh air ratio in the supplied air of the air conditioners is zero (Li et al., 2021). The patrons are represented as solid obstacles with a uniform body-surface heat release rate of 50 W/m^2 as used in the work by Wang et al. (Wang et al., 2021). For an index patient that has symptoms such as coughing, sneezing etc., and the peak exhalation speeds can be high, reaching 10–50 m/s (Bahl et al., 2022). However, as the index patient in this study did not display symptoms during the infection event, the pulmonary ventilation rate is assumed to be 1.38 m^3/h, which is the equivalent for people undergoing light exercise or speaking (Buonanno G., Morawska L. et al., 2020). The exhaled breath of the index patient is modelled as a CFD inlet (an area that releases respired air as a continuous air flow) with dimensions of 0.2 m wide and 0.2 m high at the location of index patient's head, representing pulmonary ventilation at a location with a certain small distance from the mouth of index patient. This approach is appropriate for the investigated infection event, in which the index patient was talking normally.

In order to estimate the infection probability, a target volume adjacent to the nose of an individual patron with dimensions of 0.16 m wide, 0.20 m deep and 0.2 m high is defined In order to estimate the infection probability, a target volume adjacent to the nose of an individual patron is specified. In reality, the target volume would vary in size depending on physical features of the patron and would vary in location as the head of the patron moved. Given that the patrons remain at their tables for the entire exposure, for simplicity it is assumed that the target volumes remain static in location and are uniform in size with dimensions of 0.16 m wide (representing the approximate width of a face), 0.20 m high (representing the approximate height of a face) and has a depth of 0.2 m from the face. For seated patrons, the centre of the target volume is 1.17 m above the floor.

To investigate potential SARS-CoV-2 transmission routes and potential mitigation measures for the X restaurant infection event, the following six CFD scenarios were simulated:

Scenario 1: The aerosol scenario (with particle size of 1 μm diameter) with a low ventilation rate (4.9 ACH) as defined in Table 2.

Scenario 2: The base case scenario, utilising the multi-droplet approach with eight droplet groups (droplets up to 40 μm diameter) and a low ventilation rate (4.9 ACH) as defined in Table 2.

Scenario 3: A scenario similar to Scenario 2 but including nine droplet groups (with droplets up to 45 μm) for droplet size sensitivity analysis.

Scenario 4: A scenario similar to Scenario 2 but with a higher ventilation rate (19.5 ACH).

Scenario 5: A scenario similar to Scenario 2 but with table partitions included.

Scenario 6: A scenario similar to Scenario 2 but with a higher ventilation rate (19.5 ACH) and table partitions included.

All the CFD predictions presented in this paper were produced using a computational mesh consisting of 983,326 (229 × 38 × 113) cells. Using a computer with a 4.0 GHz four-core processor and 64 GB of memory and a time step size of one second, it required approximately 125 h to simulate one 82-minute exposure scenario including eight particle groups and 134 h for one scenario including nine particle groups, compared with 76 h for the gas tracer approach. A mesh sensitivity study was performed using two meshes for the base case scenario, a coarse mesh of 983,326 (229 × 38 × 113) cells and a finer mesh of 2,557,500 (330 × 50 × 155) cells (see SM Section S4 for details). Both mesh scenarios produced similar patterns and magnitudes of air flow speeds, quanta distributions in the air and reasonably good agreement of individual infection probability. While reproducing the observed 9 secondary infections in the RIR, the overall predicted secondary infections are 10.71 when using the coarse mesh and 10.95 when using the fine mesh, with a relative difference of just 2 %. Considering the high computational time cost for the fine mesh (308 h) and the small difference in the predicted secondary infections, the coarser mesh is used in all the six simulations in the main paper.

Table 1
The droplet size, mass contribution, deposition velocity and filtration efficiency for air conditioner filters.

Particle	Size range (μm)	<5	5–10	10–15	15–20	20–25	25–30	30–35	35–40
	Representative diameter (μm)	2.5	7.5	12.5	17.5	22.5	27.5	32.5	37.5
Mass composition (mass fraction) (Xie et al., 2009)		8E-5	0.010	0.032	0.047	0.086	0.170	0.297	0.358
Deposition velocity (m/s) (Giardina and Buffa, 2018)		1E-4	0.003	0.01	0.02	0.03	0.04	0.06	0.10
Filtration efficiency (%) (Li et al., 2021; Anozie, 2020)		5	60	95	95	95	95	95	95

Table 2
Key parameters defining the CFD model.

Parameter	Value	Note
Geometry	See Fig. 1. Ceiling height is 3.14 *m*	Details from Li et al. (Li et al., 2021).
Walls	0.1 m thick	With default wall material properties in SMARTFIRE (Ewer, 2017).
Natural ventilation	A 0.6 × 0.2 m^2 vent at the bottom of stair door	The stair door and lift to the restaurant opened for approximately 3 s every two minutes (Li et al., 2021). Considering these openings are far from the index (at table A), only a small vent is set at the bottom of the stair door and the ventilation from the lift is ignored.
Exhaust fan	A 0.3 × 0.3 m^2 air vent with a flow rate of 0.072 m^3/s	This flow rate refers to the natural air change rate (Li et al., 2021).
Air conditioning	Total air change rate of 4.9 ACH The air conditioners are assumed to be 2 m above the floor. Three large air conditioner units are represented with three 1.6 × 0.1 m^2 inlets located 0.5 m from the wall and a flow rate of 0.16 m^3/s; two small air conditioner units include 1.0 × 0.1 m^2 inlets with a flow rate of 0.1 m^3/s. Filtration efficiency as reported in Table 1 No fresh air is supplied Temperature 17 ^{O}C	The configuration of the air conditioners including the air inlet/outlet in the X restaurant can be found in (Lu and Yang, 2020). As the event occurred during the very early stages of the pandemic, a low air ventilation rate is assumed. The overall filtration efficiency is reported to be 20 % (Li et al., 2021). Referring to (Li et al., 2021).
Room temperature	20 ^{O}C	
Pulmonary ventilation rate	1.38 m^3/h	For light exercise or speaking (Buonanno G., Morawska L., 2020).
Droplet mass fraction in the respirated air stream produced by the index patient	0.1	The absolute value is not critical because, as seen in Equation (9), it is scaled to 1 for quanta concentration calculation.
Patrons	Represented as a set of solid obstacles. A heat release rate of 50 W/m^2 is applied to the body surfaces of all people.	Referring to (Wang et al., 2021).
Index inlet	A 0.2 × 0.2 m^2 high inlet at the head location with a continuous 1.38 m^3/h flow rate.	Represents the air that has been exhaled from the nose/mouth of the index patient.
Particle density	1000 kg/m^3	Water density.
Aerosol size	1 μm	
Deposition velocity for aerosol	0.0001 m/s for horizontal surface and clothes	Using the data for sticky wood surface (Giardina and Buffa, 2018). Also, see Table 1.
Target volume for quanta concentration	For individual patrons, the simulated quanta concentration is taken as the average value within a volume 0.16 m wide, 0.20 m deep and 0.2 m high, adjacent to the susceptibles nose.	Used in the inhaled quanta calculation.
Mesh (cells)	983,326 (229 × 38 × 113) cells	See SM Sec S4 for mesh sensitivity analysis.
Timestep size (s)	1	

4.2. Methodology employed to estimate secondary infections

The methodology used to estimate the secondary infections for the X restaurant is described in this section. For the two different approaches used to simulate the virus laden respiratory flow (i.e., the tracer gas and the multi-size droplet approaches), the aerosol/droplet concentrations are first predicted by performing the CFD simulations with the model setup summarised in Table 1 and 2. The aerosol/droplet transportation is modelled using Eqs. (4) to (8).

The aerosol/droplet concentration in each target volume (i.e., the volume representing the nose area of the susceptible as described in Section 4.1) is averaged over the volume. The quanta concentration in each target volume is then calculated from Eq. (9) using the average aerosol/droplet concentration in the volume. The infection probability for the susceptible associated with its target volume is calculated using Eq. (12). Zhang et al. (Zhang et al., 2021) have analysed the infection risk via fomites and close contact by observing more than 40,000 surface touches and 13,000 episodes of close contacts in the X restaurant during the entire lunch session. While patrons were observed to spend 90.6 % of their time touching surfaces while dining, patrons touched mucous surfaces (eyes, nostrils, lips) on average only once per hour. And the number of times patrons who were infected during the X restaurant dining session touched mucous surfaces was only one seventh that for the non-infected patrons sitting at the same table. On this basis, Zhang et al. ruled out virus transmission via fomites contact and interpersonal close contact routes. Therefore, the number of quanta contributed from fomites contact, a in Eq. (12) is assumed to be 0 for the infection probability calculation.

The quanta generation rate for the investigated infection event in the X restaurant is unknown. It is thus back calculated from the known number of infections in this event. The target is to determine the quanta generation rate that can produce nine secondary infections within the RIR. The iterative method used to determine the expected quanta generation rate is depicted in the flow chart presented in Fig. 3. This is

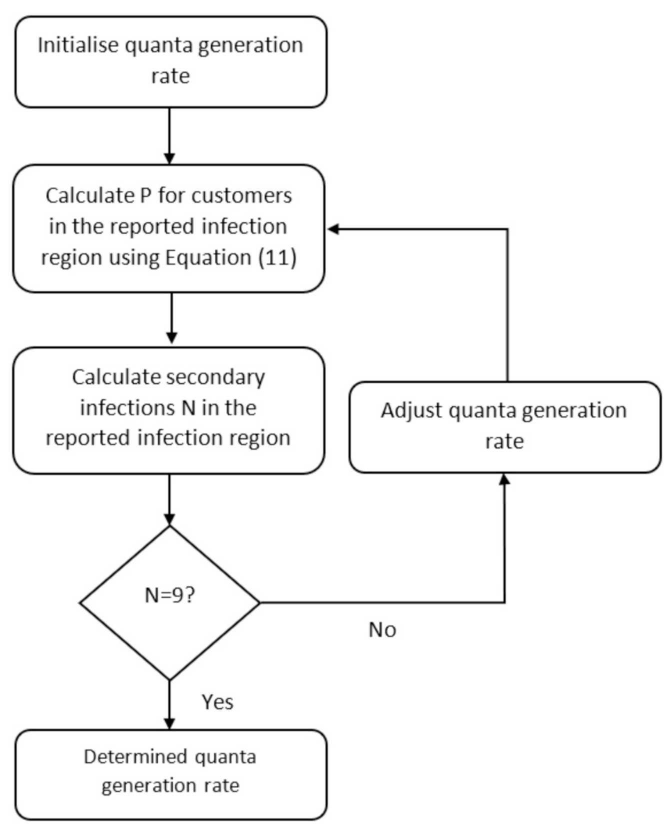

Fig. 3. Flow chart for the back calculation of the quanta generation rate.

achieved by modifying the quanta generation rate and comparing the estimated secondary infections with the known number of secondary infections. This back calculation is only applied to the RIR where the secondary infections occurred. With the back-calculated quanta generation rate, the secondary infections in the other part of the restaurant (i.e., RNIR) are then estimated.

Using this approach, the back-calculated quanta generation rate for the aerosol approach is 226 quanta/h, while for the multi-size droplet approach, the quanta generation rate is 2520 quanta/h. It is noted that the quanta generation rate required to produce the nine secondary infections in the RIR for the aerosol approach is an order of magnitude smaller than that for the multi-size droplet approach. This is to be expected as in the multi-size droplet approach, many of the larger particles drop out of the airflow before infecting susceptibles, whereas in the aerosol approach, most of the particles remain in the airflow and so can infect susceptibles. Thus, fewer quanta are required in the aerosol approach. Using these back calculated quanta generation rates, the estimated secondary infections predicted by the two different approaches is described in Section 4.3 and presented in Table 3.

4.3. Simulation results and secondary infections

The actual exposure durations with exposure starting times for the susceptibles at each table in the transmission event (Li et al., 2021) are presented in Table 3. The exposure starting times for the index patient and the susceptibles, who arrived earlier, are denoted as time zero. The exposure periods after the index patient left the restaurant were 14 min for susceptibles at table 8, 5 min for table 10, 7 min for table 15 and 56 min for table 17. The index patient spent 82 min in the restaurant. As the CFD simulations start from the arrival of the index patient and end after 82 min, the exposure after 82 min for susceptibles at these four tables are not considered. However, in reality infections can occur for some time after the index patient has left the environment since aerosolised respiratory particles can remain suspended in the air. Thus, assuming the maximum exposure time for all susceptibles in this study is 82 min is considered a reasonable assumption for the multi-sized particle approach, but is likely to result in an underestimation of the number of secondary infections for the aerosol approach (see discussion in Section 4.3.2).

4.3.1. Simulation predictions based on the aerosol approach

The surface quanta concentrations (see Fig. 4a), and the concentrations in a horizontal plane 1.17 m above the floor (see Fig. 4b), at the end of the simulation period (i.e., after 82 min), as determined using the aerosol approach are depicted in Fig. 4. The height of 1.17 m corresponds to the centre of the target volume used to estimate infection probability for each seated susceptible. The height is intended to represent the nominal location of the nose of each susceptible. The height of 1.17 m corresponds to the centre of the target volume used to estimate infection probability for each seated susceptible. The height is intended to represent the nominal location of the nose of each susceptible. As seen in Fig. 4b, the quanta concentrations at nose height in the restaurant gradually decrease with increased distance from table A, where the index patient was seated. The average quanta concentration (based on the value experienced by each person seated at the table) decreases from an average value of approximately 0.4 quanta/m^3 for those seated at table A to approximately 0.29 quanta/m^3 for those seated at table 9, the furthest table away from the index patient. For this case, only 62.4 of the 226 released quanta (i.e., 27.6 %) deposit on surfaces. The inhaled quanta during the exposure for five susceptibles i.e., A3 (one of the infected susceptibles), 18–1, 15–1, 11–1 and 9–1 located at table A, table 18, table 15, table 11 and table 9 respectively (See Fig. 1 for the seating locations of the identified susceptibles) are depicted in Fig. 5. Among these five susceptibles, A3 has the highest quanta inhalation (0.82). Susceptible 9–1 has the minimum (0.45), which is slightly more than half of the quanta inhalation for A3. As a result, as seen in Fig. 4(c), the predicted infection probabilities decrease from 51 %–56 % at table A to 23 %–38 % at table 9. As seen in Table 3, while the aerosol modelling approach correctly predicts that number of secondary infections within the RIR i.e., 8.99 compared with the reported 9, it significantly overpredicts the ***total*** number of secondary infections – predicting 32.3 compared with only 9 in the actual event i.e., overpredicting by 259 %. The aerosol approach predicts 23.3 secondary infections in the RNIR where none were actually reported, which is similar to the estimation of 22.0, based on the tracer gas experimental data derived from the work of Li et al. (Li et al., 2021), described in Section 2.2. Furthermore, the number of the secondary infections at table 9, which is the farthest table from the index patient and located in the RNIR, is 3.42 which is comparable with the predicted secondary infections at table A (4.80) and table C (2.20) both of which are located in the RIR. Thus, the aerosol approach significantly fails to reproduce the distribution of secondary infections in this infection event.

Table 3
Reported secondary infections and estimations using the aerosol/droplet approaches.

Table	Number of Seated Susceptibles	Starting time of exposure (min)	Exposure duration (min)	Secondary infections		
				Aerosol approach (Scenario 1)	Droplet approach (Scenario 2)	Reported
A	9	0	82	4.80	5.41	4
B	4	0	53	1.99	1.38	3
C	7	2	77	2.20	2.21	2
Region total	20	NA	NA	8.99	9.00	9
5	2	0	79	0.87	0.15	0
6	4	0	82	1.77	0.12	0
7	3	0	69	0.54	0.01	0
8	2	27	69	0.72	0.01	0
9	10	0	75	3.42	0.07	0
10	6	5	82	2.56	0.11	0
11	7	0	70	2.20	0.09	0
12	2	0	64	0.62	0.02	0
13	6	0	50	1.35	0.02	0
14	3	0	61	0.90	0.05	0
15	8	0	89	3.72	0.22	0
16	5	0	48	1.16	0.08	0
17	5	59	79	1.19	0.25	0
18	5	0	77	2.30	0.51	0
Region total	68	NA	NA	23.31	1.71	0
Total	88	NA	NA	32.3	10.71	9

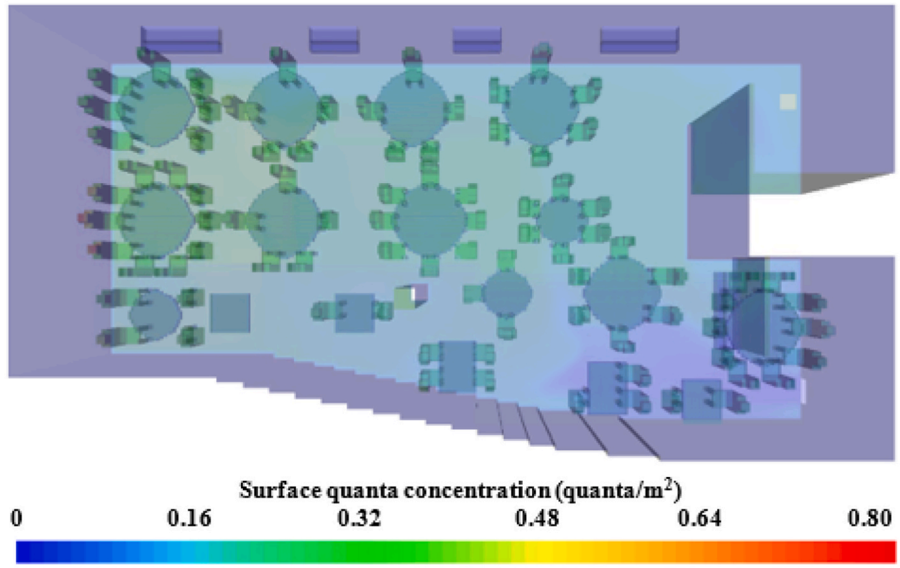

(a)

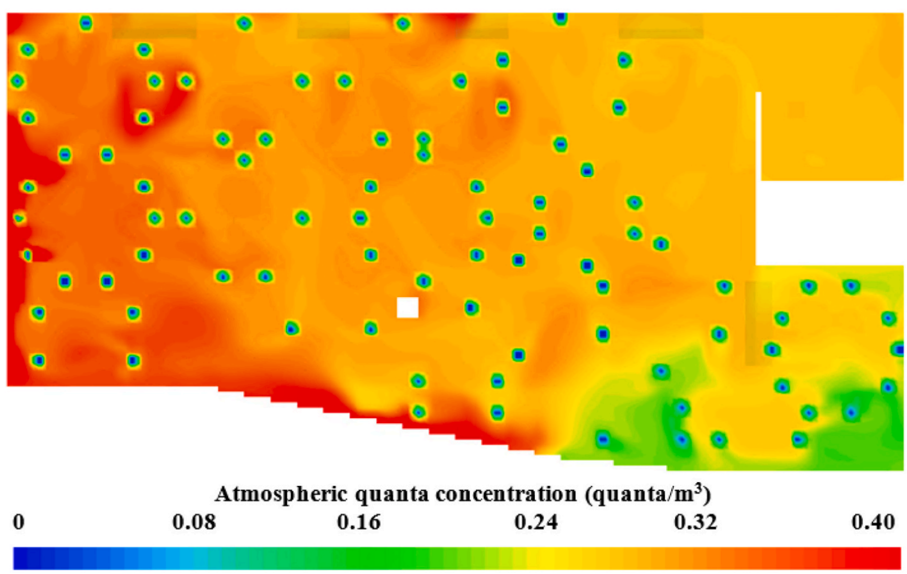

(b)

Fig. 4. Simulated quanta concentrations (a) on surfaces represented using a perspective view and (b) on a horizontal plane 1.17 m above the floor (i.e., nose-height) at the end of the aerosol simulation (Scenario 1) and (c) the infection probabilities (%) for individual patrons (location of the index patient (A1) and location of actual secondary infections (black circles)).

4.3.2. Simulation predictions based on the multi-size droplet approach

Predicted quanta concentrations on surfaces (see Fig. 6a) and in a horizontal plan at nose-height (see Fig. 6b) at the end of the multi-size droplet simulation (i.e., after 82 min) (Scenario 2) are depicted in Fig. 6. Using the multi-size droplet approach, very high levels of quanta concentration are predicted on surfaces and in the air in the RIR, where the nine reported secondary infections were seated (see Fig. 6). Furthermore, as depicted in Fig. 6b, the quanta air concentrations at nose height sharply decrease just a short distance from the index patient, with quanta concentrations outside the RIR being almost zero. While there were more infections at table B in the infection event than at table C, the predicted quanta concentrations at table C are slightly higher than at table B. This difference is due to the modelled heat release and resulting thermal plumes rising from the seated diners (see Fig. S9 for the impact of body heat plumes on the air flow pattern) and the modelled ventilation rate. However, there is uncertainty in the modelled heat release rate, thermal plumes and ventilation which is further compounded by the uncertainty in the precise seating location of each of the diners. In the multi-size droplet simulation, during the time that the index patient is in the restaurant, 2310 of the 2520 released quanta (i.e., 91.7 %) deposit on surfaces. As seen in Fig. 6(c), the predicted infection probabilities at table A are as high as approximately 90 %. The infection probabilities sharply decrease to a low value of approximately 0.8 % at table 9.

It is noted that the prediction of infection risk is only considered up to the time that the index patient leaves the restaurant (i.e., a total of 82 min). Assuming that after the index patient leaves the restaurant, any remaining patrons are then exposed to the predicted airborne concentration of respiratory droplets/aerosols at 82 min, the estimated secondary infections are 34.9 for the aerosol approach and 11.34 for the

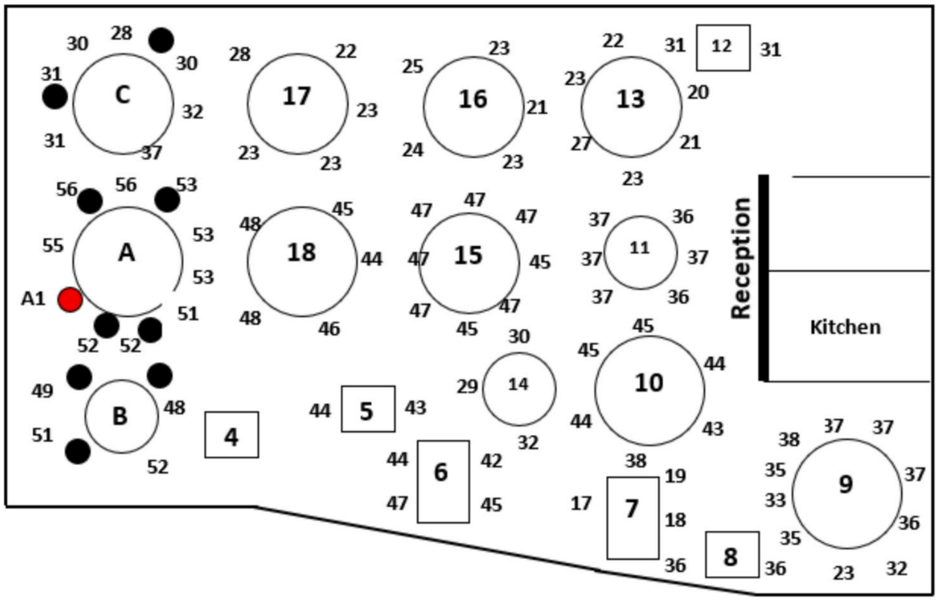

Fig. 4. (*continued*).

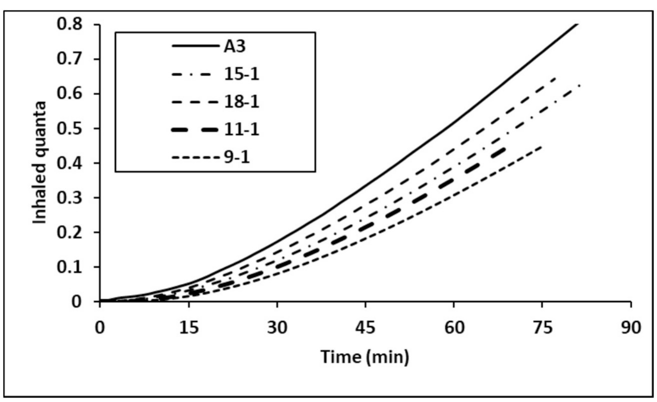

Fig. 5. Cumulative inhaled quanta predicted by the aerosol approach (Scenario 1) from the arrival of the index patient as function of time for susceptible at individual tables.

multi-droplet approach. This implies that the predicted secondary infections presented in Table 3 are probably underestimated by a maximum of 2.6 or 8 % for the aerosol approach and by 0.63 or 6 % for the multi-droplet approach. For the aerosol approach, this prediction error of 8 % is considered a reasonable approximation as the aerosol particles remain airborne for a relatively long period of time. However, in the multi-droplet approach, the airborne droplet concentration of these larger particles decays rapidly due to deposition once the index patient has left the restaurant. Thus, after 82 min, very few respiratory particles are likely to be left airborne and so the number of secondary infections is unlikely to increase significantly. Therefore, for the multi-droplet approach, the prediction error for the number of secondary infections presented in Table 3 would be much smaller than 0.63 or 6 %.

The inhaled quanta for susceptibles A3 and 18–1 (see Fig. 1 for their seating locations), during their exposure are depicted in Fig. 7. Susceptible 18–1 is one of the susceptibles in the RNIR sitting closest to the RIR. As demonstrated by the predicted quanta distribution at nose height (see Fig. 6b), the inhaled quanta by susceptibles, over the duration of the exposure, decreases sharply with distance from the index patient (see Fig. 7). The inhaled quanta, as predicted by the multi-size droplet approach, drops sharply from 2.04 quanta for susceptible A3 seated at table A, to 0.15 quanta for susceptible 18–1 seated at table 18 (see Fig. 7). The inhaled quanta for susceptible 9–1, who is located farthest from the index patient, is just 0.007. As a result, the total number of secondary infections predicted using the multi-droplet approach is 10.71, compared to 9.0 in the actual incident, an over-estimation of 19 %, with only 1.71 secondary infections predicted in the RNIR of the restaurant (Table 3).

Thus, the predicted secondary infection distribution derived using the multi-size droplet approach more closely matches the observed infection transmission than the prediction using the aerosol approach. The difference between the predictions produced by the two different modelling approaches for the secondary infection rate in the restaurant, is mainly due to the multi-size droplet approach simulating the transport of larger virus laden particles while the aerosol approach assumes that the larger respiratory droplets evaporate and become aerosols carried by the air currents. This suggests that the assumption of larger droplets shrinking to aerosols within seconds due to evaporation may not be valid and that the transmission of SARS-CoV-2 in the X restaurant is likely to be via larger respiratory droplets.

4.3.3. *Factors influencing the extent of the reported infection region*

Airflow streamlines produced by a CFD simulation of the recirculating air within the X restaurant suggests that the arrangement of the air conditioning units within the restaurant produced five air recirculation zones as depicted in Fig. 8. Zone 1 corresponds to the RIR. While aerosols are able to be transferred from Zone 1 to Zone 2 and even as far as Zone 5 (see Fig. 4), larger droplets are essentially constrained to Zone 1 by the airflow. The ventilation pattern within the X restaurant behaves as a barrier for the larger droplets, effectively preventing the transfer of the larger droplets from one zone to another as seen in Fig. 6.

This study suggests that there are two significant factors that influence the nature of the infection region in the X restaurant transmission event. The first factor is the nature of the flow produced by the air conditioning units within the restaurant (see Fig. 8). The second factor is that the infection transmission route is driven by the dispersion of larger respiratory droplets. Previous studies by Li et al (i.e., the tracer gas experiment and CFD simulations using 5 μm droplets) (Li et al., 2021) and by Liu et al. (i.e., CFD simulations using 1.5 μm droplets) (Liu et al., 2021) only identified the specific flow pattern in the X restaurant as being responsible for the infection event but overlooked the importance of the larger droplets in defining the reported infection region and in predicting a reasonable estimate of the **total** number of secondary

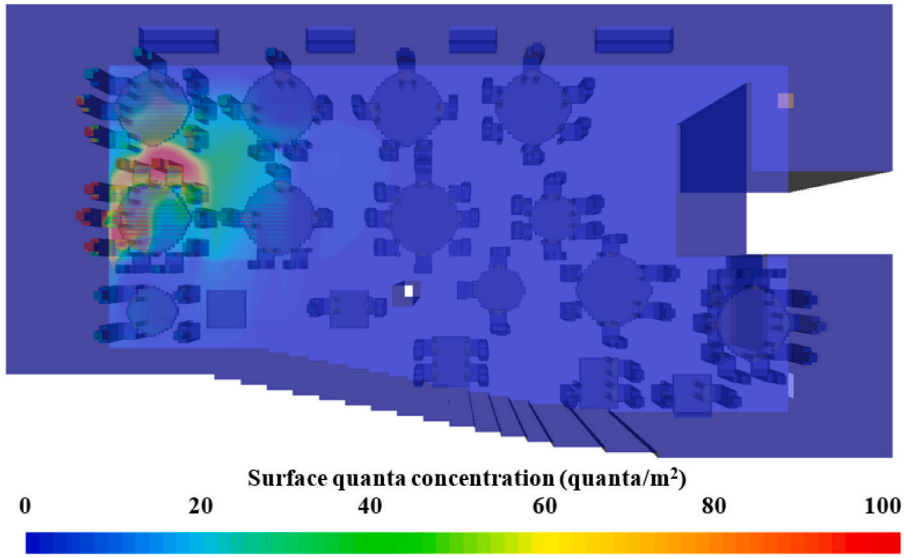

(a)

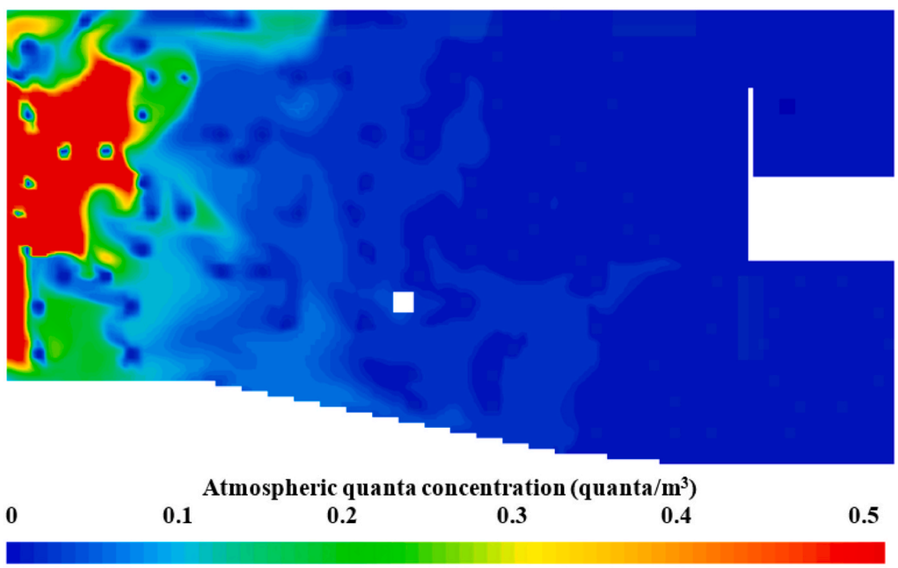

(b)

Fig. 6. Simulated quanta concentrations (a) on surfaces and (b) on a horizontal plane 1.17 m above the floor (i.e., nose-height) at the end of the multi-size droplet simulation (Scenario 2) and (c) the infection probabilities (%) for individual patrons (location of the index patient (A1) and location of actual secondary infections (black circles)).

infections.

5. Discussion

5.1. Transmission routes

The finding in the current study, that the transmission of SARS-CoV-2 in the X restaurant is likely via the larger respiratory droplets, would initially appear to contradict the conclusions of the work by Xu et al. (Xu et al., 2024). The model developed by Xu et al. (Xu et al., 2024) to describe the X restaurant infection event, incorporated four infectious disease transmission routes: short-range airborne, long-range airborne, fomite and large droplet. Their model was supported by analysis of surveillance video from the actual infection event, including real data concerning close contact and surface touch behaviours. Based on this analysis, Xu et al. concluded that the infection risk for the diners was due to a combination of mechanisms, with short-range airborne contributing 28.1 %, long-range airborne contributing 60.3 %, the fomite route contributing 11.6 % and with the large droplets making a negligible contribution. However, the large droplets in the work by Xu et al. assumed a threshold of 75–100 μm. For these large droplets to significantly contribute to the predominant infection route would require the index patient to be within 0.2 m (for talking) or 0.5 m (for coughing) of a susceptible. For the investigated infection event, the index patient was not observed to cough and susceptible close encounters with the index patient of less than 0.2 m are negligible (Xu et al., 2024). It should be noted that the larger sized droplets considered in the current study have diameters of up to 40 μm. Thus, the larger droplet route considered in the current study is within the categories of short-range airborne and long-range airborne in the analysis by Xu et al. Therefore, the finding in the current study is in fact consistent with the conclusions from Xu et al.

Feng et al. (Feng et al., 2024) analysed the X restaurant infection

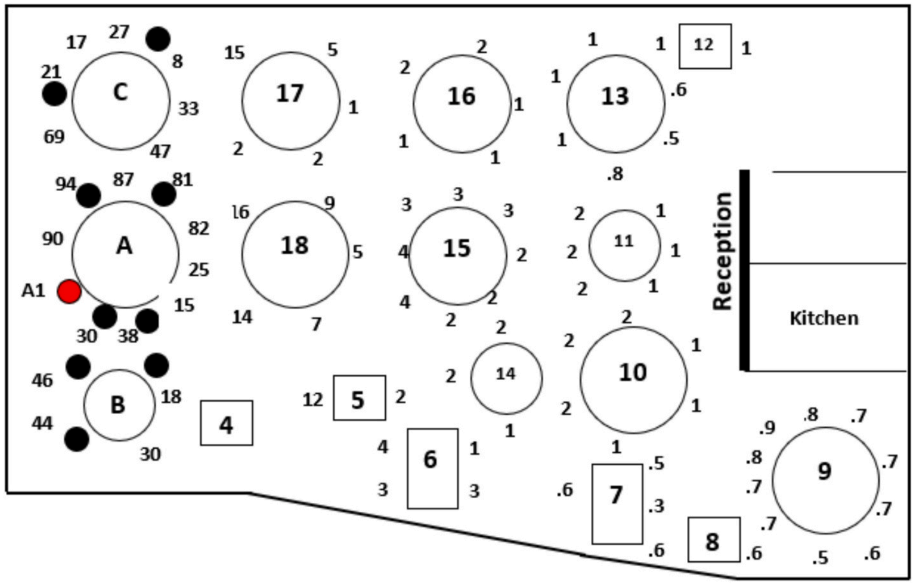

(c)

Fig. 6. (*continued*).

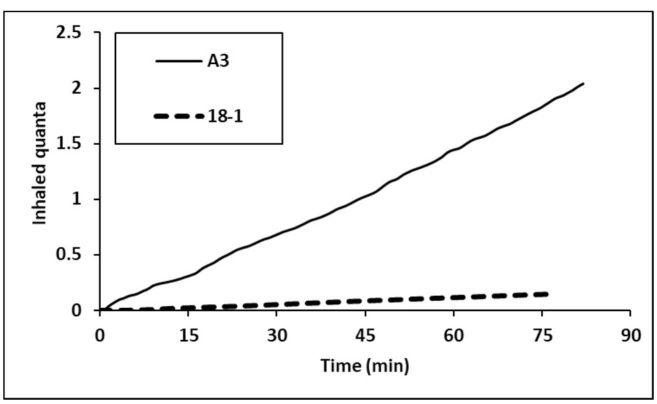

Fig. 7. Cumulative inhaled quanta from the arrival of the index patient as function of time for susceptibles at individual tables in Scenario 2.

event using a probability analysis that made use of a modified Wells-Riley model and explored the impact of combining both short-range (less than 2 m) and room-scale (more than 2 m) effects. In their analysis, particles with a size of <50 μm are considered for infections in the short-range zone, which is similar to that in the current study (i.e., <40 μm), and 5 μm for infections in the long-range zone. Rather than using a back-calculated quanta generation rate for the X restaurant infection event, their quanta generation rate was derived from Monte Carlo simulations using general quanta generation distribution data from the literature. As a result, their analysis only predicted 3.0 secondary infections on average for the short range (<2 m) and 1.5 secondary infections for the long range for the respiratory and air conditioner filtration scenarios they investigated, and so failed to reproduce the observed secondary infection distribution within the X restaurant event.

5.2. *Back calculated quanta generation rates*

As noted in Section 4.2, there is a significant difference between the back calculated quanta generation rates for the aerosol approach in Scenario 1 (226 quanta/h) and the multi-size droplet approach in Scenario 2 (2520 quanta/h). Furthermore, the quanta generation rate of

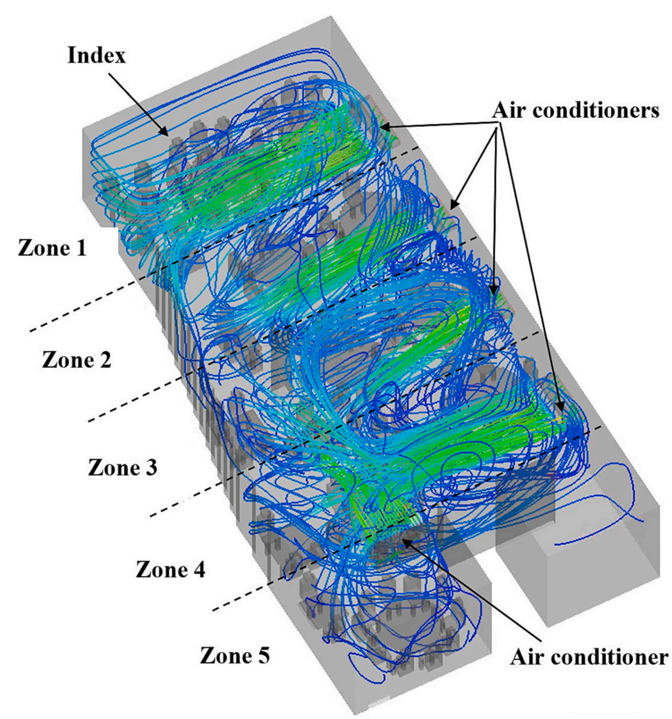

Fig. 8. Streamlines originating from the air conditioning units in Scenario 2.

2520 quanta/h appears very large compared with other studies for Covid-19 transmissions (Buonanno G., Morawska L. et al., 2020; Buonanno G., Stabile L. et al., 2020). In the simulations using the aerosol approach, most of virus laden aerosols are suspended in the air. However, with the multi-size droplet approach, 91.7 % of the released quanta deposit on solid surfaces and hence only 8.3 % of the released quanta are suspended in the air. This is equivalent to a quanta generation rate of 210 quanta/h taking into consideration only the quanta suspended in the air. This quanta generation rate is comparable to that reported for super-spreading cases (Buonanno G., Morawska L. et al., 2020; Buonanno G., Stabile L. et al., 2020; Miller et al., 2021; Wang et al., 2021).

5.3. Sensitivity of droplet size

In the multi-size droplet approach described in Section 4, the droplet sizes used in the simulation of Scenario 2 had a maximum size of 40 μm (see Table 1). The simulation shows that droplets up to this size can be transported from the index patient to the neighbouring tables, B and C. As a result, the number of predicted secondary infections in the RNIR (i.e., 1.71) are much lower than that predicted using the aerosol approach (i.e., 23.3) and much closer to that reported in the actual incident (i.e., zero). In this section, the sensitivity of the number of predicted secondary infections in the RNIR is analysed with a simulation (Scenario 3) involving droplets up to 45 μm. The droplet sizes and corresponding mass compositions are presented in SM Section S3, Table S2. The deposition velocity of droplets with size of 40–45 μm is 0.14 m/s and the filtration efficiency for the air conditioner is assumed to be the same as that for other large droplets as seen in Table 1, i.e. 95 %. When the maximum droplet size is 45 μm, the estimated secondary infections in the RNIR are 1.62, a decrease of 0.09 persons or 5 %. Therefore, for the investigated restaurant transmission, droplets with size up to 40 μm are considered adequate to reflect the transmission behaviour.

It should be noted that the distance that moderately large respiratory droplets can be transported, depends on the speed of the air flow produced by the ventilation inside the restaurant. Even when the air flow is relatively weak (approximate 0.1–0.4 m/s), moderately large droplets (in the range of approximately up to 40 μm) can be transported by the air flow for a short but potentially significant distance beyond the index patient before they fall to a horizontal surface. Therefore, for a restaurant scenario in which moderately large droplets can possibly travel to neighbouring tables, either due to high ventilation rates or small table separation, they cannot be ignored in analysis of Covid-19 transmission.

5.4. Impact of mucous membrane contact

In the analysis in Section 4, based on the findings of the X restaurant analysis by Zhang et al. (Zhang et al., 2021) and Xu et al. (Xu et al., 2024), the fomite quanta contribution to the infection probability is ignored. The small, but non-zero number of secondary infections predicted in the RNIR for simulations including larger droplets is possibly due to the exclusion of a fomite transmission route. An experimental study by Ding et al. (Ding et al., 2022) suggests that deposited respiratory droplets on dining plates could be the dominant viral transmission route when a diner shared a table with an infected person. In another experimental study, Walkers et al. (Walker et al., 2022) found that the transfer of fomites from surfaces to hand (i.e., the fomite transfer efficiency) was less than 10 % via surface touching if the relative humidity is 40 %. However, the fomite transfer efficiency increased markedly as humidity increased, reaching a maximum of approximately 50 % for the fomites on the surfaces. Besides touching the eyes, nose and mouth with hands, fomites can also be directly transferred from surfaces of dining cutlery such as forks and knives, spoons, water glasses etc. to the mouth or lips during the dining period. In addition to inhaled aerosols, Saulnier et al. suggest that the oral viral transmission route represents a strong candidate and the amount of infectious virus in large droplets deposited on intermediate vectors such as glasses, beverages, cutlery and food on plates must be considered in restaurant environments (Saulnier et al., 2023). As seen in Fig. 6(a), very high quanta concentrations are on the surface of tables, patrons' clothes, and the floor within the reported infection region. Therefore, if the deposited quanta also somehow contribute to the secondary infections in the reported infection region, the back calculated quanta generation rate would be less than the 2520 quanta/h calculated in Section 4.2 without considering the fomites contact. Correspondingly, the estimated secondary infections in the RNIR would be less than the 1.71 persons reported in Table 3.

To investigate the impact of the transmission via fomites contact, it is assumed that the deposited quanta on a portion of the dining table surface is completely absorbed by a patron seated at the table (i.e., 100 % transfer efficiency). For a given patron, the relevant portion of the dining table surface is that part of the table adjacent to the patron and corresponds to the portion of the table they are likely to touch. Presented in Fig. 9 is the back-calculated quanta generation rate and corresponding number of secondary infections in the RNIR assuming different sizes of the relevant table surface from which the patron absorbs fomites. With a touched surface area of 0.016 m^2, or approximately a hand size (Zhang et al., 2021), the back-calculated quanta generation rate is 1135 quanta/h, resulting in the estimated number of secondary infections reducing to 1.11 persons in the RNIR. If the area of the touching region is increased by a factor of just over 3 (resulting in an area of 0.05 m^2), the absorption of quanta from the touching region results in the number of predicted secondary infections in the RNIR reducing to approximately 0.87 persons. It is noted that further increases in surface area size of the touching region does not significantly reduce the number of predicted secondary infections in the RNIR.

5.5. Mitigation measures

There are many potential mitigation measures that could be introduced to reduce the number of secondary infections in the X restaurant, including social distancing (Chu et al., 2020; CDCP, 2020; HM Government, 2021), high ventilation rates (Li et al., 2021; Morawska et al., 2020), table partitions (Patankar, 1980; Ye et al., 2021) and shortened exposure time (Wang et al., 2021); these are explored in this section.

5.5.1. Social distancing

By reviewing and analysing the data from 38 observational studies, Chu et al. concluded that the infection probability of SARS-CoV-2 would decrease from 12.8 % for situations in which the index and susceptible were separated by a short physical distance (less than 1 m) to 2.6 % with a separation distance of more than 1 m and that a separation of 2 m is a more effective mitigation (Chu et al., 2020). The 2 m social distancing mitigation was adopted worldwide as a means to help prevent the spread of SARS-CoV-2 (CDCP, 2020; HM Government, 2021). The physical distance between the index patient seated at table A and each of the two secondary infections seated at table C in the X restaurant infection event was 3.6 m and 4.6 m (Li et al., 2021). These distances are 80 % and 130 % greater, respectively, than the commonly employed 2 m social distancing mitigation. Thus, imposing a 2 m social distancing policy would not have prevented these two secondary infections within the X restaurant environment. However, if a 2 m social distancing policy was employed in the X restaurant without changing the table arrangements, there would be just two patrons per table. With 18 tables, the occupancy would be reduced from the 89 to 36, with just six seated patrons in the RIR, the index patient and five susceptibles and 30 susceptibles seated in the RNIR. Using the average infection probability at each table

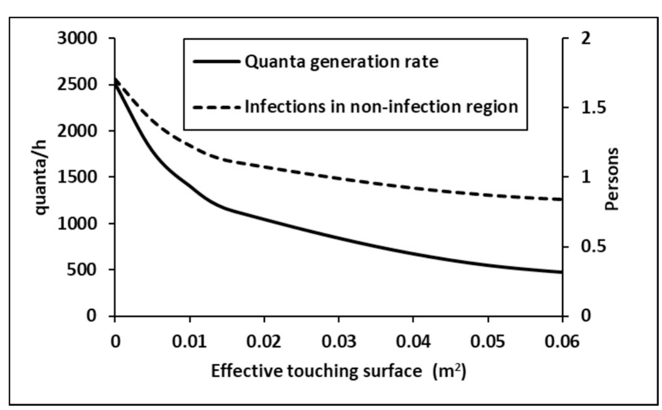

Fig. 9. Back-calculated quanta generation rate and estimated secondary infections in the reported non-infection region with various surface areas from which the deposited quanta are absorbed by patrons.

determined from the base case simulation (see Section 4), the estimated number of secondary infections among the five susceptibles in the RIR would be 1.89, with 0.77 amongst the 30 susceptibles in the RNIR. Thus, even with the greatly reduced number of patrons resulting from imposing a 2 m social distancing within the X restaurant, some 2.66 secondary infections are predicted amongst the 35 suceptiables, representing 7.6 % of the patrons. This compares with 10.2 % (i.e., 9 out of 88) of the susceptible population being infected if social distancing was not implemented.

5.5.2. High ventilation rate

Morawska et al. (Morawska et al., 2020) suggested the use of ventilation controls in public buildings would be an important low-cost measure to reduce the likelihood of disease transmission. Previous studies (Li et al., 2021; Zhang et al., 2021; Liu et al., 2021) suggested that the transmission of SARS-CoV-2 in the X restaurant was due to poor ventilation – however, this conclusion was influenced by the assumption that the main transmission route was via aerosols. In this section, the impact of ventilation rate on the number of secondary infections is explored numerically by increasing the ventilation rate from 4.9 ACH in Scenario 2 to 19.5 ACH Scenario 4, an increase of almost 300 %. While the air conditioning system does not supply fresh air, the filtration efficiency is assumed to be 95 % for the larger droplets considered in this study. With a high ventilation rate in Scenario 4, the ventilation barrier observed in Scenario 2 (see Section 4.3.3) is broken due to the strong crossing air recirculation established between the RIR and the RNIR (see Fig. 10). A clear air recirculation is seen with flow from the NRIR to the RIR in the lower layer and from the RIR to the RNIR at the upper layer. The simulated quanta concentrations in a horizontal plane at nose height are presented in Fig. 11. Compared with the quanta distributions produced using the lower ventilation rate (see Fig. 6), with the increase in the ventilation rate, the area with higher quanta concentrations (i.e., 0.2 quanta/m^3) extends beyond the RIR to the RNIR.

Estimated secondary infections under various air change rates, exposure durations and table partition states are compared in Table 4. With a higher ventilation rate of 19.5 ACH and maintaining the same quanta generation rate as in the case with a 4.9 ACH ventilation rate i.e., 2520 quanta/h (see Section 4), while the higher ventilation rate reduces the number of secondary infections in the RIR by 18 %, from 9 to 7.38 the predicted number of secondary infections in the RNIR increases from 1.71 to 3.40 (an increase of 99 %). Thus, rather than reducing the number of secondary infections, increasing the ventilation rate by 300 % has resulted in a slight overall increase in secondary infections of 0.7 % (see Table 4). As seen in Table 1, the filtration efficiency for particles greater than 10 μm is 95 %, which is equivalent to a supply of 95 % fresh air in the ventilation system in terms of virus removal. As seen in Fig. S11, SM Section S5, a higher ventilation rate does not necessarily result in a higher quanta removal rate i.e., the ratio of the removed quanta is not the same as the ratio of ventilation rates. Furthermore, the higher ventilation rate results in the larger droplets mixing more thoroughly compared with that for the low ventilation rate. Therefore, simply increasing the ventilation rate (or fresh air ratio) is not an effective means of reducing the transmission of SARS-CoV-2 by larger respiratory droplets within the X restaurant environment. Thus, the claim made by other studies (Li et al., 2021; Zhang et al., 2021; Liu et al., 2021) that the transmission of SARS-CoV-2 in the X restaurant was due to poor ventilation is not supported by the current study. However, it is noted that this conclusion may not be valid for all restaurant environments, which may have very different ventilation and humidity conditions compared to that of the X restaurant.

5.5.3. Table partitions

The impact of table partitions (i.e., screens) on secondary infections is also examined. The table partitions are assumed to be 1 m high with the base of the partition 0.45 m above the floor. The partitions create a square grid around the tables (see Fig. 12). The partition locations depicted in Fig. 12 are selected simply to demonstrate the potential benefits of using physical partitions to reduce infection risk without considering their potential impact on access or table service during dining. For simplicity, it is further assumed that the partition surfaces have the same particle deposition velocities adopted for the horizonal surfaces.

The predicted quanta concentration on a horizontal plane at nose height at the end of the simulation period, using the multi-sized droplet approach with table partitions, are depicted in Fig. 12. Compared with Fig. 6(b), the quanta concentrations are reduced using the partitions throughout the RNIR and table B in the RIR when using the low ventilation rate (Fig. 12(a)). Furthermore, using the low ventilation rate and the table partitions, the number of secondary infections is reduced throughout the restaurant, with the overall number of secondary infections reduced by 2.49 or 23.2 %, the number of secondary infections reduced by 1.37 or 15.2 % in the RIR and 1.12 or 65.5 % in the RNIR (see Table 4).

In contrast, with a high ventilation rate and table partitions, the quanta concentrations are reduced throughout the RIR except for table A, where the index patient is seated and slightly increase in the RNIR

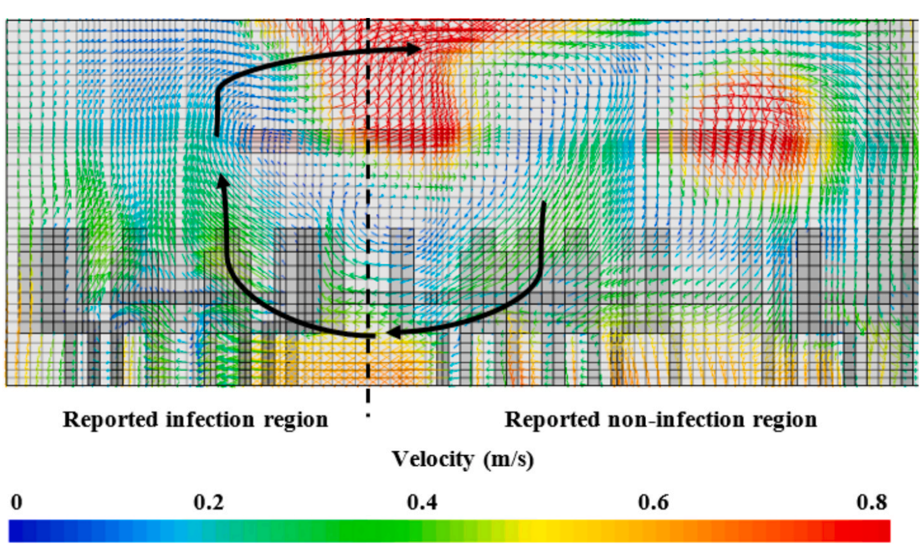

Fig. 10. Predicted velocity distribution in the longitudinal and vertical direction in the plane passing through the middle of the restaurant at the end of the simulation for Scenario 4 with a higher ventilation rate.

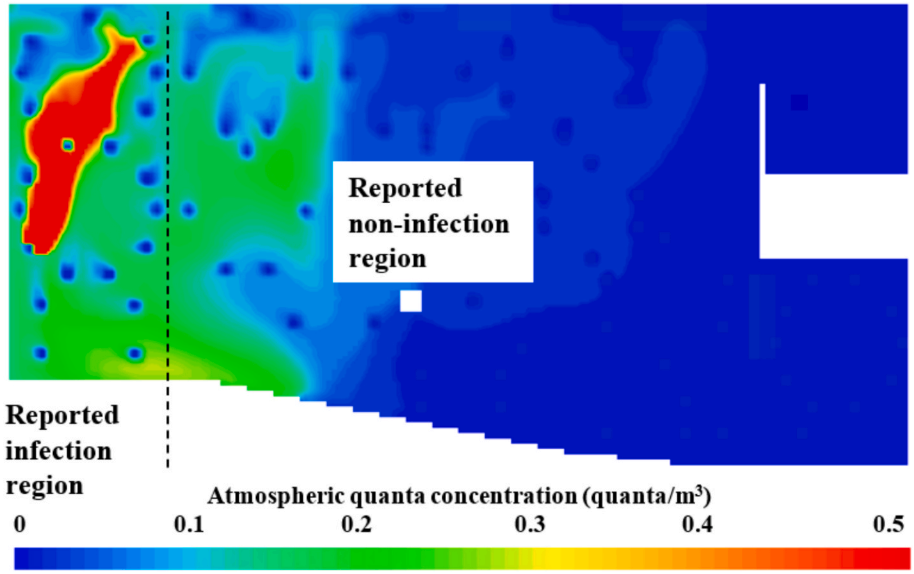

Fig. 11. Simulated quanta concentration in a horizontal plane 1.17 m above the floor (i.e., nose-height) with high ventilation rate at the end of the multi-size droplet simulation (Scenario 4).

Table 4
Estimated secondary infections under various air change rates, exposure duration and table partition states.

Air change rate (ACH)	With table partitions	Exposure duration (min)	Predicted Secondary infections			Reduction in the number of secondary infections (%)
			Reported Infection Region	Reported Non-Infection Region	Total	
		as in Table 3	9	1.71	10.71	–
	No	60	8.32	1.87	10.19	4.9
		45	6.94	1.40	8.34	22.1
		30	5.22	0.91	6.13	42.8
4.9		as in Table 3	7.63	0.59	8.22	23.2
	Yes	60	7.01	0.72	7.73	27.8
		45	5.90	0.53	6.43	40.0
		30	4.60	0.35	4.95	53.8
	No	as in Table 3	7.38	3.4	10.78	− 0.7
		as in Table 3	5.41	1.99	7.40	30.9
19.5	Yes	60	4.66	2.18	6.84	36.1
		45	3.78	1.62	5.40	49.6
		30	2.81	1.07	3.88	63.8

(Fig. 12(b)). Using the high ventilation rate and the table partitions, the overall number of secondary infections is reduced by 3.31 or 30.9 %. The number of secondary infections in the RIR is reduced by 3.59 or 40 % however, the number of secondary infections is increased by 0.28 or 16.4 % in the RNIR (see Table 4). Thus, while the higher ventilation rate alone does not reduce the number of secondary infections (see Section 5.5.2), when combined with table partitions, the overall number of secondary infections is reduced by 30.9 %.

This suggests that the use of table partitions, in addition to ventilation changes, can be an effective mitigation measure to reduce the number of secondary infections in restaurants. However, the interaction between scenario specific parameters such as, the nature of the specific ventilation flow patterns within the restaurant, the number of air changes per hour achieved, the table distribution and the nature of the table partitions, is complex, and so it is difficult to generalise on the effectiveness of individual parameters. As demonstrated by the analysis of the specific X restaurant environment, high ventilation flows combined with table partitions can result in an overall reduction in secondary infections by as much as 30 % but can increase localised secondary infection rates in one part of the restaurant by 16 %, while reducing secondary infections in other parts of the restaurant by 40 %. Similarly, with the same ventilation system and table partitions, but with lower ventilation rates, reductions in overall infection rates are slightly less at 23 %, but they are reduced throughout the restaurant.

5.5.4. *Restricting dining duration*

The specific transmission of SARS-CoV-2 via larger droplets makes conventional mitigation measures such as the use of high ventilation rates or social distancing less effective in transmission events as occurred in the X restaurant. Another potential mitigation strategy, to reduce the number of quanta inhaled and hence reduce infection risk, is to restrict potential exposure time. If the dining duration of patrons is changed from that shown in Table 3, to a uniform 60 min, 45 min and 30 min, the total number of secondary infections can be reduced by 4.9 %, 22.1 % and 42.8 % respectively, compared with the base case scenario i.e., a ventilation rate of 4.9 ACH, no table partitions and the actual dining times. If, in addition to restricting the dining times to 60 min, 45 min and 30 min, table partitions are also used, the total number of secondary infections can be further reduced by 27.8 %, 40.0 % and 53.8 % respectively. Finally, if the higher ventilation rate is used, along with table partitions and restricted dining times, the total number of secondary infections is significantly reduced by 36.1 % to 6.84, 49.6 % to 5.4 and 63.8 % to 3.88 respectively. Thus, restricting dining times of patrons would be an effective means of reducing the number of secondary infections, especially if combined with table partitions and higher ventilation rate.

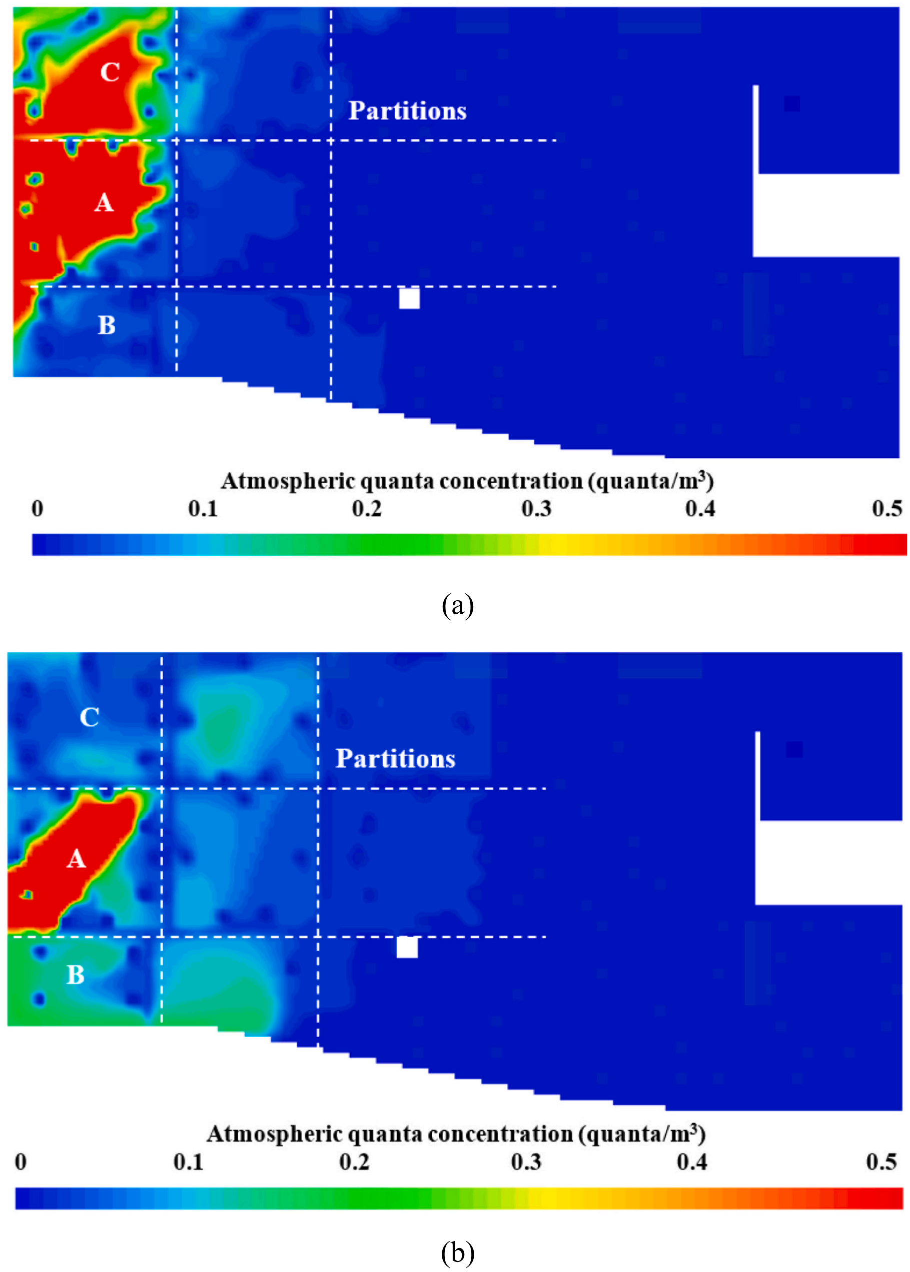

Fig. 12. Simulated quanta concentration on a horizontal plane 1.17 m above the floor (i.e., nose-height) at the end of the multi-size droplet simulation with table partitions and (a) low ventilation rate and (b) high ventilation rate.

5.6. Concerning the coupled CFD Wells-Riley modelling approach

The reliability and validity of the general approach of coupling CFD simulations with the Wells-Riley model (referred to as coupled CFD-WR model) has been questioned by Sedighi et al. [75] due to the necessity to redefine the quanta concept in these coupled models. In the original Wells-Riley model [19], a quantum is defined as the integer number of infectious airborne particles required to infect a susceptible and may comprise one or more airborne particles. Sedighi et al [75] suggest that the quanta in many of the coupled CFD-WR modelling approaches is described by a continuous variable which brings into question the validity of the approach. However, a different approach has been adopted in this study in which quanta is not a continuous variable calculated from its own transport equation. As seen in Eq. (5), droplets are represented by continuous scalars in the CFD simulation. The integer quanta (or indeed, any form of quanta) are not directly involved in the CFD simulation. The quanta concentrations are calculated from the simulated droplets mass fractions using Eq. (9). The number of integer quanta inhaled by a susceptible is characterised using the Poisson distribution with an expectation of λ (see Eq. (1)). The continuous quanta concentration derived with Eq. (9) is only used to estimate the parameter λ of the Poisson distribution, i.e. the expectation of the number of inhaled integer quanta by a susceptible. Therefore, although the coupled CFD-WR model presented in this study could be interpreted as a dose–response model, the integer nature of quanta in the original Wells-Riley model is maintained. When the coupled CFD-WR model is interpreted as a dose–response model, the quanta exposure (i.e., a continuous variable) specially refers to the average of the inhaled integer quanta (which is a random event) within a given duration by a susceptible (i.e. the expectation λ). Another concern raised by Sedighi et al., is that the coupled CFD-WR technique (or the new approach of estimating λ) has not been validated using animal-based laboratory experiments. While this is a legitimate concern, unfortunately, there are no suitable experiments available for validation purposes (Sedighi et al (Sedighi et al., 2025). However, it is suggested that the study described in this work, utilising a real and well characterised infection event is a reasonable validation of the coupled CFD-WR approach.

6. Limitations

As in any numerical investigation of a complex process, some assumptions are required to simplify the analysis and to accommodate the various uncertainties in the data. In this section, the main limitations of the work presented in this study are discussed.

- A key assumption in this study is that the time for the larger sized droplets, in the X restaurant infection event, to dry is not less than patrons' exposure time i.e., their dining times. This assumption is supported by the important finding (Pease et al., 2022) that respiratory droplets containing mucus can persist for as long as hours. However, the time to evaporate depends on the composition and amount of mucus within droplets and the humidity of the environment. Although the indoor humidity during the X restaurant infection event was unknown, the region where the restaurant is located has high humidity, with a year-average humidity of approximate 78 %. Therefore, the findings for the X restaurant might not be applicable for restaurant infection events in regions where the humidity is significantly lower. Furthermore, while the droplets have a greatly reduced evaporation rate, in the current study it was assumed, for simplicity, that the size of droplets was fixed over the duration of the infection event. Lieber et al. (Lieber et al., 2021) found that following the evaporation of the water content, a saliva droplet reaches a final size after approximately 200 s, which then remains stable for many hours. The equilibrated droplet diameters are approximately 20 %–50 % of the initial sizes, which depend on the droplet composition, and environmental conditions (temperature and humidity). Considering the likely high humidity in the investigated X restaurant, the equilibrated droplet size in the X restaurant is assumed to be one third of the initial size adopted for the analysis presented in this study. As discussed in Section 4.1, as only equilibrated droplet sizes less than 40 μm are of interest, the measured droplets with initial sizes up to 120 μm (Xie et al (Xie et al., 2009) are considered here. Fig. 13 compares the droplet mass composition used in the current study (i.e., the measured data by Xie et al. (Xie et al., 2009) with sizes up to 40 μm) and the droplet mass composition after evaporation (with initial droplet sizes up to 120 μm). As the droplet mass distribution curves in Fig. 13 are similar, this suggests that the droplet size distribution adopted in this study (without evaporation) is similar to that of the measured droplets after evaporation. Furthermore, the omission of the evaporation process (which requires approximately 200 s at most) might impact the predicted infection probability distribution within the RIR, but the impact on the infection probability within the NRIR is expected to be minor. Thus, ignoring the evaporation process is unlikely to impact the key finding in this study, i.e. the conclusion that the transmission in the X restaurant is via larger droplets.
- The air flow rates of the air conditioners in the X restaurant were unknown. While Li et al. conducted an experimental study in the X restaurant and performed numerical simulations, unfortunately, the air flow rates were not provided (Li et al., 2021). A low air ventilation rate of 4.9 ACH is adopted in this study considering the fact that the event occurred in the very early stage of the pandemic when the role of ventilation in preventing the Covid-19 spread had not been widely known. With this ventilation rate, the simulated flow pattern (see Fig. 8) is qualitatively similar to that predicted by Li et al. Furthermore, estimated secondary infections in each region, i.e., RIR and RNIR, based on the aerosol simulation in the current study (i.e., 9 and 23.3 infections respectively, see Table 3) is almost identical to that derived from experimental data using a tracer gas by Li et al. (i.e., 9 and 22.0 infections respectively, see Section 2.2).
- The ventilation mitigation explored in this work only consisted of increasing the ventilation rate of the air-conditioning system found within the X restaurant. However, the introduction of a modified ventilation system, such as a displacement approach, where air supply diffusers are located near floor level and air is extracted at ceiling level, may be able to effectively reduce infection risk.
- Within the current study, the reduction of virions due to the decay of active airborne virions over time (Lin and Marr, 2020) is not considered. Excluding this phenomenon from the analysis will result in an overestimation of infection probability. However, this impact is not significant as the exposure time in the event is not very long (less than 82 min).
- The transmission route via fomites contact is ignored in the current study. Although this simplification is supported by the findings from the investigations by Zhang et al. (Zhang et al., 2021) and Xu et al. (Xu et al., 2024), the predicted high quanta levels on solid surfaces should be taken into consideration when general mitigation strategies are considered.
- For simplicity it was assumed that the deposition velocities on the suggested vertical partitions between tables was the same as that for horizontal surfaces. Generally, the deposition velocity on a vertical surface is much lower than that on a horizontal surface if the materials for the two surfaces are identical. Therefore, the efficiency of the suggested table partition mitigation strategy is limited by the nature of the materials that constitute the partition surfaces.

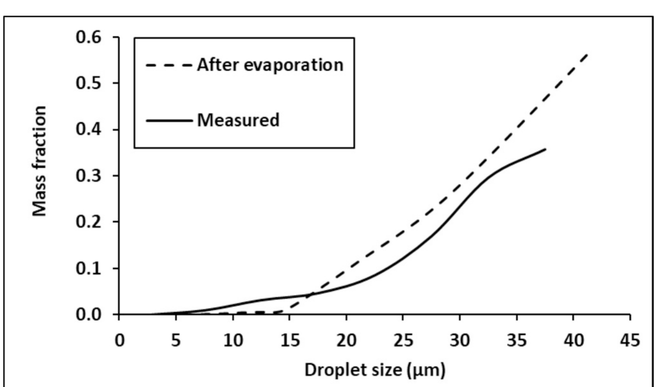

Fig. 13. Droplet mass composition used in the simulations (measured) and that with equilibrated sizes (after evaporation).

7. Conclusion

It has been suggested by previous research that the transmission of SARS-CoV-2 in the X restaurant infection event in Guangzhou China on 24th January 2020 was due to poor ventilation. This conclusion is not supported by the current study, which made use of a coupled Wells-Riley and CFD simulation, reproducing the distribution of the secondary infections in the X restaurant infection event. Earlier investigations by other researchers assumed that an aerosol treatment of the infected respiratory droplets was appropriate, with droplet sizes approximately 1 μm. This is predicated on the assumption that larger sized respiratory droplets rapidly evaporate and become aerosolised. However, it is now known that mucus rich respiratory droplets require a relatively long time to evaporate, which invalidates the assumption that the larger sized respiratory droplets, formed while patrons are dining and talking, are predominately aerosolised. Thus, the approach adopted in this study made use of the novel multi-size droplet approach and took into consideration respiratory droplets ranging in size up to 40 μm. Using this approach, a more accurate prediction of the number and location of secondary infections was achieved compared to the aerosol approach.

The main findings of the current study are:

- The SARS-CoV-2 infection event in the X restaurant is primarily the result of infection transmission via larger sized respiratory droplets, not aerosols or small droplets,
- By reproducing the reported nine secondary infections in the reported infection region, using droplets of up to 40 μm, the simulated secondary infections in the other part of the restaurant, where there were no reported secondary infections (reported non-infection region) was only 1.71.
- In contrast, a simulation based on the conventional aerosol approach, where respiratory particles are assumed to be no greater than 1 μm, predicted as many as 23.3 secondary infections in the reported non-infection region.
- Furthermore, it was demonstrated using data derived from a previous experimental study within the X restaurant, which made use of a tracer gas to represent the dispersion of respiratory aerosols, that a total of 22.0 secondary infections are predicted in the reported non-infection region.
- In addition, using CFD simulation data that made use of small droplets of not greater than 5 μm produced by other researchers in an earlier study, it is also demonstrated that as many as 6.1 secondary infections would result in the reported non-infection region.
- If larger sized infected respiratory particles are considered to be the main vector for infection within the X restaurant, high ventilation rates are not an effective mitigation in preventing the spread of COVID 19 – where a mechanical air recirculation system was in use and the air had a high humidity. If the ventilation rate is increased by 300 % (from 4.9 ACH to 19.5 ACH), the secondary infection rate does not decrease, but results in an increase of 0.7 %.
- The use of table partitions in the X restaurant transmission event is an effective mitigation measure to reduce the number of secondary infections. Even with a high ventilation rate, the use of partitions could reduce the number of secondary infections by 31 %.
- Reducing dining duration to 30 min together with a high ventilation rate and table partitions can reduce the number of secondary infections by 64 %.
- It is predicted that 91.7 % of the released quanta from the index patient deposit on surfaces such as clothes, tables and the floor, which implies a high potential risk for the transmission via fomites contact.

Therefore, for a restaurant scenario in which moderately large respiratory droplets can possibly travel to neighbouring tables, either due to ventilation or small table separation, they cannot be ignored in analysis of infection disease transmission.

Finally, given the high humidity in the X restaurant scenario, and the complex nature of the interaction between scenario specific parameters such as, the nature of the specific ventilation flow patterns, the number of air changes per hour achieved, the table distribution and the nature of the table partitions, it is difficult to generalise on the effectiveness of individual mitigation scenarios explored in this study.

However, in restaurants and other spaces involving food or beverage consumption, it is suggested that effective mitigations to reduce secondary infections during pandemics include, the use of appropriate table partitions, reducing exposure times by controlling the patron dining duration, encouraging patrons to reduce surface touching and regularly cleaning hands and object surfaces using sanitisers and for restaurant staff to regularly clean all surfaces. Furthermore, as a COVID-19 infection transmission route in restaurant environments appears to be via moderately sized respiratory particles, especially in high humidity locations, it is suggested that this provides further evidence and justification for serving staff to be masked at all times to reduce their risk of infection – as facial masks are more effective at filtering larger respiratory particles.

It is noted that droplet evaporation cannot be directly incorporated within the Eulearian CFD modelling approach adopted in this study. While the impact of excluding evaporation is considered small, to explore the potential effect of droplet evaporation on the main conclusions of the study, a further analysis using the Lagrangian CFD approach could be performed.

While the coupled CFD and Wells-Riley modelling approach is sometimes questioned due to the lack of validation using animal-based laboratory experiments, the study described in this work, utilising a real and well characterised infection event is a reasonable validation of the coupled technique.

CRediT authorship contribution statement

Zhaozhi Wang: Writing – review & editing, Writing – original draft, Visualization, Software, Methodology, Investigation, Formal analysis, Conceptualization. **Fuchen Jia:** Writing – review & editing, Writing – original draft, Visualization, Software, Methodology, Investigation, Formal analysis, Conceptualization. **Edwin R Galea:** Project administration, Resources, Supervision, Writing – review & editing, Conceptualization, Funding acquisition, Investigation. **John Ewer:** Writing – review & editing, Visualization, Methodology, Funding acquisition, Conceptualization. **Angus Grandison:** Writing – review & editing, Methodology, Formal analysis, Conceptualization.

Declaration of competing interest

The authors declare that they have no known competing financial interests or personal relationships that could have appeared to influence the work reported in this paper.

Acknowledgements

This work was partially supported by the University of Greenwich's proof of concept award [Fund Code 14621], 2021. The authors gratefully acknowledge the contribution from three anonymous reviewers who made valuable contributions to improve the clarity and quality of this work.

Appendix A. Supplementary material

Supplementary data to this article can be found online at https://doi.org/10.1016/j.ssci.2025.106938.

Data availability

The software used is not open access and is commercially available. All other data used in the paper is available from the cited references.

References

World Health Organization (WHO), WHO Coronavirus (COVID-19) Dashboard. https://covid19.who.int. (Accessed 18 January 2025).

Cheung, H., Kumar, P., Hama, S., et al., 2024. Monitoring of indoor air quality at a large sailing cruise ship to assess ventilation performance and disease transmission risk. Sci. Total Environ. https://doi.org/10.1016/j.scitotenv.2024.178286.

Fisher, K.A., Tenforde, M.W., Feldstein, L.R., et al., 2020. Community and close contact exposures associated with COVID-19 among symptomatic adults ≥18 years in 11 outpatient health care facilities — United States, July 2020. Morb. Mortal. Wkly Rep. 69 (36), 1258–1264. https://doi.org/10.15585/mmwr.mm6936a5.

Pray, I.W., Kocharian, A., Mason, J., et al., 2021. Trends in outbreak-associated cases of COVID-19 — Wisconsin, March–November 2020. Morb. Mortal. Wkly Rep. 70 (4), 114–117. https://doi.org/10.15585/mmwr.mm7004a2.

Lu, J., Gu, J., Li, K., et al., 2020. COVID-19 outbreak associated with air conditioning in restaurant, Guangzhou, China, 2020. Emerg. Infect. Dis. 26 (7), 1628–1631. https://doi.org/10.3201/eid2607.200764.

Li, Y., Qian, H., Hang, J., et al., 2021. Probable airborne transmission of SARS-CoV-2 in a poorly ventilated restaurant. Build. Environ. 196. https://doi.org/10.1016/j.buildenv.2021.107788.

Kwon, K.S., Park, J.I., Park, Y.J., et al., 2020. Evidence of long-distance droplet transmission of SARS-CoV-2 by direct air flow in a restaurant in Korea. J. Korean Medical Sciences 35. https://doi.org/10.3346/jkms.2020.35.e415.

Capon, A., Houston, J., Rockett, R., 2021. Risk factors leading to COVID-19 cases in a Sydney restaurant. Aust. N. Z. J. Public Health 45, 512–516. https://doi.org/10.1111/1753-6405.13135.
Cheng, V.C., Lung, D.C., Wong, S., et al., 2022. Outbreak investigation of airborne transmission of Omicron (B.1.1.529)-SARS-CoV-2 Variant of concern in a restaurant: implication for enhancement of indoor air dilution. J. Hazard. Mater. 430. https://doi.org/10.1016/j.jhazmat.2022.128504.
Jia, W., Wang, Q., Lung, D., et al., 2024. Co-existence of airborne SARS-CoV-2 infection and non-infection in three connected zones of a restaurant. J. Hazard. Mater. 480. https://doi.org/10.1016/j.jhazmat.2024.136388.
Zhang, N., Hu, T., Zhang, J., et al., 2022. Probable close contact transmission in a restaurant in China. J. Infect. 85, 573–607. https://doi.org/10.1016/j.jinf.2022.08.029.
Greenhalgh, T., Jimenez, J.L., Prather, K.A., et al., 2021. Ten scientific reasons in support of airborne transmission of SARS-CoV-2. Lancet 397 (10285), 1603–1605. https://doi.org/10.1016/S0140-6736(21)00869-2.
Meyerowitz, E.A., Richterman, A., Gandhi, R.T., et al., 2020. Transmission of SARS-CoV-2: a review of viral, host, and environmental factors. Ann. Intern. Med. https://doi.org/10.7326/M20-5008.
Kampf, G., Brüggemann, Y., Kaba, H., et al., 2020. Potential sources, modes of transmission and effectiveness of prevention measures against SARS-CoV-2. J. Hospital Inf. 106 (4), 687–697. https://doi.org/10.1016/j.jhin.2020.09.022.
Drossinos, Y., Weber, T., Stilianakis, N., 2021. Droplets and aerosols: an artificial dichotomy in respiratory virus transmission. Health Sci. Rep. 4. https://doi.org/10.1002/hsr2.275.
World Health Organization. (2024). Indoor airborne risk assessment in the context of SARS-CoV-2: description of airborne transmission mechanism and method to develop a new standardized model for risk assessment. World Health Organization. https://iris.who.int/handle/10665/376346.
Reid, J., Ferro, A., Finn, A., et al., 2024. World Health Organization report removes the aerosol/droplet dichotomy but does not move us forward in infection control strategies. Aerosol Sci. Tech. 58. https://doi.org/10.1080/02786826.2024.2387985.
Wells, W., 1955. In: Airborne Contagion and Air Hygiene. Cambridge University Press, Cambridge MA, pp. 117–122.
Riley, E.C., Murphy, G., Riley, R.L., 1978. Airborne spread of measles in a suburban elementary school. Am. J. Epidemiol. 107, 421–432. https://doi.org/10.1093/oxfordjournals.aje.a112560.
Patankar, S., 1980. Numerical heat transfer and fluid flow. Intertext Books. McGraw Hill, New York.
Hathway, E.A., Noakes, C.J., Sleigh, P.A., et al., 2011. CFD simulation of airborne pathogen transport due to human activities. Build. Environ. 46, 2500–2511. https://doi.org/10.1016/j.buildenv.2011.06.001.
Peng, S., Liu, Q.E., 2020. The role of computational fluid dynamics tools on investigation of pathogen transmission: prevention and control. Sci. Total Environ. 746. https://doi.org/10.1016/j.scitotenv.2020.142090.
Mirzaie, M., Lakzian, E., Khan, A., et al., 2021. COVID-19 spread in a classroom equipped with partition – a CFD approach. J. Hazard. Mater. 420. https://doi.org/10.1016/j.jhazmat.2021.126587.
Wang, Z., Galea, E.R., Grandison, A., et al., 2021. A coupled computational fluid dynamics and Wells-Riley model to predict COVID-19 infection probability for passengers on long-distance trains. Saf. Sci. 147. https://doi.org/10.1016/j.ssci.2021.105572.
Zhu, S., Srebric, J., Spengler, J.D., et al., 2012. An advanced numerical model for the assessment of airborne transmission of influenza in bus microenvironments. Build. Environ. 47, 67–75. https://doi.org/10.1016/j.buildenv.2011.05.003.
Yan, Y., Li, X., Shang, Y., et al., 2017. Evaluation of airborne disease infection risks in an airliner cabin using the Lagrangian-based Wells-Riley approach. Build. Environ. 121, 79–92. https://doi.org/10.1016/j.buildenv.2017.05.013.
Zhang, N., Chen, X., Jin, T., et al., 2021. Evidence for lack of transmission by close contact and surface touch in a restaurant outbreak of COVID-19. *J. Inf.* 83, 207–216. https://doi.org/10.1016/j.jinf.2021.05.030.
Liu, H., He, S., Shen, L., et al., 2021. Simulation-based study of COVID-19 outbreak associated with air-conditioning in a restaurant. Phys. Fluids 33. https://doi.org/10.1063/5.0040188.
Stettler, M.E.J., Nishida, R.T., Oliveira, P.M., et al., 2022. Source terms for benchmarking models of SARS-CoV-2 transmission via aerosols and droplets. R. Soc. Open Sci. 9. https://doi.org/10.1098/rsos.212022.
Chong, K.L., Ng, C.S., Hori, N., 2021. Extended lifetime of respiratory droplets in a turbulent vapor puff and its implications on airborne disease transmission. Phys. Rev. Lett. 126. https://doi.org/10.1103/PhysRevLett.126.034502.
Lieber, C., Melekidis, S., Koch, R., et al., 2021. Insights into the evaporation characteristics of saliva droplets and aerosols: Levitation experiments and numerical modeling. J. Aerosol Sci 154. https://doi.org/10.1016/j.jaerosci.2021.105760.
Pease, L.F., Wang, N., Kulkarni, G.R., et al., 2022. A missing layer in COVID-19 studies: transmission of enveloped viruses in mucus-rich droplets. Int. Commun. Heat Mass Transf. 131. https://doi.org/10.1016/j.icheatmasstransfer.2021.105746.
Chen, F., Yu, S.C.M., Lai, A.C.K., 2006. Modeling particle distribution and deposition in indoor environments with a new drift-flux model. Atmos. Environ. 40, 357–367. https://doi.org/10.1016/j.atmosenv.2005.09.044.
Hu, X., Jia, F., Wang, Z., Galea, E.R., 2017. Grouping methods for MPS soot transport model and its application in large-scale enclosure fires. Fire Saf. J. 9, 361–370. https://doi.org/10.1016/j.firesaf.2017.03.045.
Overholt, K.J., Floyd, J.E., Ezekoye, O.A., 2016. Computational modelling and validation of aerosol deposition in ventilation ducts. Fire Technol. 52, 149–166. https://doi.org/10.1007/s10694-014-0414-5.
Ewer J., Jia F., Grandison A., Galea E. R. and Patel M. K., *SMARTFIRE V4.4 User Guide and Technical Manual*, Fire Safety Engineering Group, University of Greenwich, UK, 2017.
Wang, Z., Jia, F., Galea, E.R., et al., 2017. A forensic analysis of a fatal fire in an indoor shooting range using coupled fire and evacuation modelling tools. Fire Saf. J. 91, 892–900. https://doi.org/10.1016/j.firesaf.2017.03.029.
Grandison, A.J., Galea, E.R., Patel, M.K., et al., 2006. A suggested procedure for benchmarking fire field models. Int. J. Eng. Performance-Based Fire Codes 8 (4), 132–144.
Wang, Z., Jia, F., Galea, E.R., et al., 2001. Simulating one of the CIB W14 round robin test cases using the SMARTFIRE fire field model. Fire Saf. J. 36 (7), 661–677. https://doi.org/10.1016/S0379-7112%2801%2900018-2.
Galea, E.R., 1989. On the field modelling approach to the simulation of enclosure fires. J. Fire. Prot. Eng. 1 (1), 11–22. https://doi.org/10.1177/104239158900100103.
Hu, X., Wang, Z., Jia, F., Galea, E.R., Patel, M.K., 2011. Simulating smoke transport in large scale enclosure fires using a multi-particle-size model. Fire Saf. Sci. 10, 445–458. https://doi.org/10.3801/IAFSS.FSS.10-445.
Liljegren, J.C., Brown, D.F., Lunden, M.M., et al., 2016. Particle deposition onto people in a transit venue. Health Security 14, 237–249. https://doi.org/10.1089/hs.2016.0010.
Buonanno, G., Morawska, L., Stabile, L., 2020. Quantitative assessment of the risk of airborne transmission of SARS-CoV-2 infection: prospective and retrospective applications. Environ. Int. 145. https://doi.org/10.1016/j.envint.2020.106112.
Buonanno, G., Stabile, L., Morawska, L., 2020. Estimation of airborne viral emission: quanta emission rate of SARS-CoV-2 for infection risk assessment. Environ. Int. 141. https://doi.org/10.1016/j.envint.2020.105794.
Miller, S.L., Nazaroff, W.W., Jimenez, J.L., et al., 2021. Transmission of SARS-CoV-2 by inhalation of respiratory. Indoor Air 31 (2), 314–323. https://doi.org/10.1111/ina.12751.
Wang, Z., Galea, E.R., Grandison, A., Ewer, J., Jia, F., 2021. Inflight transmission of COVID-19 based on experimental aerosol dispersion data. J. Travel Med. 28. https://doi.org/10.1093/jtm/taab023.
Pease, L.F., Wang, N., Salsbury, T.I., et al., 2021. Investigation of potential aerosol transmission and infectivity of SARS-CoV-2 through central ventilation systems. Build. Environ. 197. https://doi.org/10.1016/j.buildenv.2021.107633.
Marcus, L.J., et al., 2020. Assessment of Risks of SARS-CoV-2 transmission during air travel and non-pharmaceutical interventions to reduce risk, Phase one report: gate-to-gate travel onboard aircraft. Faculty and Scientists at the Harvard T.H. Chan School of Public Health. National Preparedness Leadership Initiative, Cambridge, MA 02238, USA. https://cdn1.sph.harvard.edu/wp-content/uploads/sites/2443/2020/10/HSPH-APHI-Phase-One-Report.pdf.
Volz, E., Mishra, S., Chand, M., et al., 2021. Transmission of SARS-CoV-2 Lineage B.1.1.7 in England: insights from linking epidemiological and genetic data. medRxiv. https://doi.org/10.1101/2020.12.30.20249034.
Dagpunar, J., 2021. Interim estimates of increased transmissibility, growth rate, and reproduction number of the Covid-19 B.1.617.2 variant of concern in the United Kingdom. *medRxiv*. https://doi.org/10.1101/2021.06.03.21258293.
Allen, H., Vusirikala, A., Flannagan, J., et al., 2022. Household transmission of COVID-19 cases associated with SARS-CoV-2 delta variant (B.1.617.2): national case-control study. The Lancet Regional Health - Europe 12. https://doi.org/10.1016/j.lanepe.2021.100252.
Campbell, F., Archer, B., Laurenson-Schafer, H., et al., 2021. Increased transmissibility and global spread of SARS-CoV-2 variants of concern as at June 2021. Euro. Surveill. 26. https://doi.org/10.2807/1560-7917.ES.2021.26.24.2100509.
Classification of Omicron (B.1.1.529): SARS-CoV-2 variant of concern, Worl Health Orgnization, 26 11 2021. https://www.who.int/news/item/26-11-2021-classification-of-omicron-(b.1.1.529)-sars-cov-2-variant-of-concern [Accessed 17 February 2022].
Silcott D, Kinahan S, Santarpia J, et al., TRANSCOM/AMC commercial aircraft cabin aerosol dispersion tests, Submitted to: United States Transportation Command (USTRANSCOM) & Air Mobility Command (AMC), 2020. 17 Nov 2020. Scott Air Force Base, Illinois, USA. https://www.ustranscom.mil/cmd/docs/TRANSCOM%20Report%20Final.pdf.
Wells, W., 1934. On air-borne infection: study II. droplets and droplet nuclei. Am. J. Epidemiol. 20, 611–618. https://doi.org/10.1093/oxfordjournals.aje.a118097.
Average humidity in Guangzhou. https://weather-and-climate.com/average-monthly-humidity-perc,guangzhou,china [Accessed 07 June 2022].
Xu, Z., Zhang, H., Zhu, M., et al., 2024. Human behavior-based COVID-19 transmission in two dining spaces. J. Hazard. Mater. 480. https://doi.org/10.1016/j.jhazmat.2024.135820.
Xie, X., Li, Y., Sun, H., Liu, L., 2009. Exhaled droplets due to talking and coughing. J. R. Soc. Interface 6, 703–714. https://doi.org/10.1098/rsif.2009.0388.focus.
Giardina, M., Buffa, P., 2018. A new approach for modeling dry deposition velocity of particles. Atmos. Environ. 180, 11–22. https://doi.org/10.1016/j.atmosenv.2018.02.038.
Anozie, P., RDG Guidance: Maintenance of on-train HVAC modules & filters during the COVID-19 pandemic, V1.1, Rail Delivery Group, UK, 26th May, 2020.
Lai, A.C.K., Nazaroff, W.W., 2000. Modeling indoor particle deposition from turbulent flow onto smooth surfaces. J. Aerosol Sci 31, 463–476. https://doi.org/10.1016/S0021-8502(99)00536-4.
Bahl, P., Doolan, C., Silva, C., et al., 2022. Airborne or droplet precautions for health workers treating coronavirus disease 2019? J. Infect. Dis. 225. https://doi.org/10.1093/infdis/jiaa189.
Lu, J., Yang, Z., 2020. COVID-19 Outbreak associated with air conditioning in restaurant, Guangzhou, China, 2020. Emerg. Infect. Dis. 26 (11), 2789–2791. https://doi.org/10.3201/eid2611.203774.

Feng, Y., Fan, Y., Luo, X., et al., 2024. A Wells-Riley based COVID-19 infectious risk assessment model combining both short range and room scale effects. Build. Simul. 17, 93–111. https://doi.org/10.1007/s12273-023-1060-y.

Ding, S., Lee, J.S., Mohamed, M.A., Ng, B.F., 2022. Infection risk of SARS-CoV-2 in a dining setting: deposited droplets and aerosols. Build. Environ. 213. https://doi.org/10.1016/j.buildenv.2022.108888.

Walker, M.D., Vincent, J.C., Benson, L., et al., 2022. effect of relative humidity on transfer of aerosol-deposited artificial and human saliva from surfaces to artificial finger-pads. Viruses 14 (5). https://doi.org/10.3390/v14051048.

Saulnier A., Wendling J., Hermant B., et al., 2023. SARS-CoV-2 transmission modes: Why and how contamination occurs around shared meals and drinks?, *Food Microbiol.*, Volume 114. doi: 10.1016/j.fm.2023.104297.

Chu, D., Akl, E., Duda, S., et al., 2020. Physical distancing, face masks, and eye protection to prevent person-to-person transmission of SARS-CoV-2 and COVID-19: a systematic review and meta-analysis. Lancet 395. https://doi.org/10.1016/S0140-6736(20)31142-9.

Social distancing: keep a safe distance to slow the spread, July 6, 2020, Centres for Disease Control and Prevention, USA. https://stacks.cdc.gov/view/cdc/90522. (Accessed 19 January 2025).

Social Distancing Review: Report. HM Government, UK, 2021. https://assets.publishing.service.gov.uk/government/uploads/system/uploads/attachment_data/file/999413/Social-Distancing-Review-Report.pdf. (Accessed 19 January 2025).

Lin, K., Marr, L.C., 2020. Humidity-dependent decay of viruses, but not bacteria, in aerosols and droplets follows disinfection kinetics. Environ. Sci. Technol. 54 (2), 1024–1032. https://doi.org/10.1021/acs.est.9b04959.

Coldrick, S., Kelsey, A., Ivings, M.J., et al., 2022. Modeling and experimental study of dispersion and deposition of respiratory emissions with implications for disease transmission. Indoor Air. 32. https://doi.org/10.1111/ina.13000.

Morawska, L., Tang, J., Bahnfleth, W., et al., 2020. How can airborne transmission of COVID-19 indoors be minimised? Environ. Int. 142. https://doi.org/10.1016/j.envint.2020.105832.

Ye, J., Ai, Z., Zhang, C., 2021. A new possible route of airborne transmission caused by the use of a physical partition. *J. Build. Eng.* 44. https://doi.org/10.1016/j.jobe.2021.103420.

Sedighi, A., Nardell, E., Nasiri, F., Haghighat, F., 2025. Revisiting the Wells-Riley airborne infection model: a critical analysis of its use and misuse. Build. Environ. 280. https://doi.org/10.1016/j.buildenv.2025.113136.